Journal of Scientific Computing (2020) 84:9
https://doi.org/10.1007/s10915-020-01255-4

Continuous Galerkin and Enriched Galerkin Methods with Arbitrary Order Discontinuous Trial Functions for the Elliptic and Parabolic Problems with Jump Conditions

Andreas Rupp[1] · **Sanghyun Lee**[2]

Received: 7 January 2020 / Revised: 14 April 2020 / Accepted: 8 June 2020 / Published online: 23 June 2020

Abstract
In this paper, a new version of the enriched Galerkin (EG) method for elliptic and parabolic equations is presented and analyzed, which is capable of dealing with a jump condition along a submanifold Γ_{LG}. The jump condition is known as Henry's law in a stationary diffusion process. Here, the novel EG finite element method is constructed by enriching the continuous Galerkin finite element space by not only piecewise constants but also with piecewise polynomials with an arbitrary order. In addition, we extend the proposed method to consider new versions of a continuous Galerkin (CG) and a discontinuous Galerkin (DG) finite element method. The presented uniform analyses for CG, DG, and EG account for a spatially and temporally varying diffusion tensor which is also allowed to have a jump at Γ_{LG} and gives optimal convergence results. Several numerical experiments verify the presented analyses and illustrate the capability of the proposed methods.

Keywords Enriched Galerkin method · Continuous Galerkin · Discontinuous Galerkin · Jump condition · Henry's law · Arbitrary enrichment

Mathematics Subject Classification 65M60 · 65N30

Submitted to the editors DATE.

✉ Sanghyun Lee
lee@math.fsu.edu

Andreas Rupp
andreas.rupp@fau.de

[1] Interdisciplinary Center for Scientific Computing (IWR), Heidelberg University, Mathematikon, Im Neuenheimer Feld 205, 69120 Heidelberg, Germany

[2] Department of Mathematics, Florida State University, 208 Love Building 1017 Academic Way, Tallahassee, FL 32306-4510, USA

1 Introduction

Describing flow in porous media which involves jump conditions at interfaces due to different physical properties is one of the interesting applications of this work. Several applications include coupling subsurface and overland flows [28], incompressible two-phase flows with different densities [1], different compartments within cells and different cells themselves [11], and different phases within concrete [23]. In addition, the well known Henry's law is often employed to model these jump conditions, e.g. describing the phase transition between the aqueous and the gas states of oxygen at thermodynamic equilibrium, under low pressure gradients, and for low concentrations of ions [24,26].

In this study, we focus on finite element methods that ensure robust approximations provided jump conditions in the domain. First of all, we provide a modified continuous Galerkin finite element method to preserve the accuracy of the approximation with the jump conditions (i.e. Henry's law). Secondly, we extend the idea and consider an enriched Galerkin (EG) discretization, which provides local mass conservation. The standard EG method composes of the classical continuous Galerkin (CG) function space of the polynomial order k augmented by a piece-wise constant at the center of each element [3,18,29]. EG has the same interior penalty type bi-linear form as the interior penalty discontinuous Galerkin (DG) method and it inherits many advantages of DG. However, EG has fewer degrees of freedom (DOF) than the DG method. The EG method has been developed to solve general elliptic and parabolic problems with dynamic mesh adaptivity [17,19–21] and extended to address multiphase fluid flow problems [14,21]. Recently, the EG method has been applied to solve the non-linear poroelastic problem [6,13], and its performance has been compared to other two- and three-field formulation methods [12].

The novelties of this work is first to establish a numerical scheme that allows the classical continuous Galerkin method to accurately approximate the solution with jumps in both, the primary unknown and the diffusion coefficient. (For an alternative approach to this using unfitted finite elements refer to [22] and the references therein.) Moreover, we extend the study to the EG methods for the case that local mass conservation is necessary and allow for an arbitrary degree of enrichment ultimately also covering the DG case. The optimal a priori error estimates and the stability of the method for solutions sufficing predefined jump conditions are established. This additionally allows to infer the consequences of higher order enrichment. Thus, the main objective and the novelty of this study is to provide an uniform scheme, uniform numerical analyses, and an uniform computational framework for the CG, DG, and EG methods.

The novel projection operator used in the analysis is a direct and uniform generalization of both, the standard L^2 projection (classically used in DG analysis) and the interpolation (classically used in the analysis of CG). This operator allows the sharp estimates that uniformly cover the CG, DG, and EG schemes. Moreover, it gives insights to differences in the local mass conservation property of the schemes and allows to gain (explicit) bounds for stability of the method, since it includes mass correction terms that are for example utilized for flux correction and stabilizing methods, cf. [16]. This projection, however has the drawback that it does not directly allow for optimal (with respect to the needed regularity of the time derivative) estimates in the parabolic case, because it is not L^2 orthogonal. This issue is familiar in hybrid discontinuous Galerkin (HDG) schemes [4]. Here, we bypass this issue by constructing a general L^2 projection and show the optimal convergence in the parabolic case based on both projections and exploiting their respective advantages. The basic idea is based on the analysis conducted in [24,25] for the local and hybridizable discontinuous Galerkin

methods. To this end, our analysis may serve as basis for flux correction schemes for EG, higher order enrichment where necessary (since this poses the possibility to conserve higher order momenta), and for optimal semi-discrete parabolic estimates that use L^2 orthogonality arguments (also for standard finite elements).

For the sake of simplicity, the work focuses mainly on the analysis of schemes that efficiently allow to approximate solutions with jump conditions on polygonally bounded domains. However, the scheme in (3.3) can as well—with only slight but technical modifications—be used if the interface comprising the jump conditions is not aligned with the mesh, but smooth. Moreover, our approach can be extended to curved domains by employing the isogeometric elements, and several extensions considering extended finite elements (XFEM), cut cell techniques, interface approximation techniques [5] can be applied to the method, but it is out of the main scope of this manuscript.

The paper is structured as follows: in Sect. 2, we start by describing the elliptic stationary problem and define what we understand by the terms *solution* and *regularity* when we consider jump conditions. Afterwards we construct a stable and convergent EG discretization of this problem in Sect. 3. Section 4 presents the stability analysis and we prove the optimal order of convergence estimates in the elliptic case. The previous results are extended to the parabolic diffusion equation with jump conditions in Sect. 5. In Sect. 6, several numerical experiments are presented to verify the analyses and to illustrate the performance of the proposed method. The conclusion and final remarks with possible future research prospects are included in Sect. 7.

2 Stationary Elliptic Problem

First, we analyze an EG method for a stationary diffusion problem on a bounded Lipschitz domain $\Omega \subset \mathbb{R}^d$ (with $d \leq 3$), which is assumed to be subdivided into two open, disjoint, non-degenerated Lipschitz polytopes Ω^ℓ, Ω^g such that $\overline{\Omega} = \overline{\Omega}^\ell \cup \overline{\Omega}^\mathrm{g}$. We assume $\partial\overline{\Omega}$ to be disjointly subdivided into Γ_D and Γ_N denoting the Dirichlet and Neumann boundaries, respectively. Moreover, $\Gamma_\mathrm{LG} := \partial\Omega^\ell \cap \partial\Omega^\mathrm{g}$ is the interface between Ω^g and Ω^ℓ where the Henry jump condition (cf. [27, Sec. 2.4.2]) with solubility constant H^{Γ_LG} is supposed to hold. For an illustration, the reader is referred to Fig. 6. Then the problem is formulated as

$$\begin{cases} -\nabla\cdot(D\nabla u) = f & \text{in} \quad \Omega^\ell \cup \Omega^\mathrm{g}, \\ u_\ell/u_\mathrm{g} = H^{\Gamma_\mathrm{LG}} & \text{on} \quad \Gamma_\mathrm{LG}, \\ D_\ell\nabla u_\ell\cdot\boldsymbol{\nu}_\ell + D_\mathrm{g}\nabla u_\mathrm{g}\cdot\boldsymbol{\nu}_\mathrm{g} = 0 & \text{on} \quad \Gamma_\mathrm{LG}, \\ -D\nabla u\cdot\boldsymbol{\nu} = g_\mathrm{N} & \text{on} \quad \Gamma_\mathrm{N}, \\ u = u_\mathrm{D} & \text{on} \quad \Gamma_\mathrm{D}, \end{cases} \tag{2.1}$$

for given $f \in L^2(\Omega)$, uniformly symmetric positive definite $D \in W^{1,\infty}(\Omega^\ell \cup \Omega^\mathrm{g})^{d,d}$, $u_\mathrm{D} \in H^1(\Omega^\ell \cup \Omega^\mathrm{g})$ (sufficing the jump condition at Γ_LG), $g_\mathrm{N} \in H^1(\overline{\Omega})$, and $H^{\Gamma_\mathrm{LG}} \in \mathbb{R}^+$. Moreover, u_α and D_α denote the restrictions of the respective functions to Ω^α in this work. Here, $\boldsymbol{\nu}_\alpha$ denotes the outward unit normal with respect to Ω^α ($\alpha = \ell, \mathrm{g}$) and $\boldsymbol{\nu}$ is the outward unit normal with respect to Ω.

Remark 2.1 1. D being uniformly symmetric positive definite implies the existence of a constant $C_D \geq 1$ (independent of $\mathbf{x} \in \Omega^\ell \cup \Omega^\mathrm{g}$) such that for all $\boldsymbol{\xi} \in \mathbb{R}^d$

$$C_D^{-1}\|\boldsymbol{\xi}\|_2^2 \leq \boldsymbol{\xi}\cdot D\boldsymbol{\xi} \leq C_D\|\boldsymbol{\xi}\|_2^2.$$

This also implies $C_D \geq \|D(t,\cdot)\|_{L^\infty(\Omega^\ell\cup\Omega^\mathrm{g})}$.

2. The flux is $\mathbf{q} := -D\nabla u$ and it's *continuity* across Γ_{LG} ensures conservation of mass, while the primary unknown u can be interpreted as concentration of a chemical species or a pressure depending on the considered application.

Next, we state the assumptions for a weak solution of the above problem (2.1) as following:

Definition 2.2 (*Weak solution and regularity*) A weak solution of (2.1) on the domain Ω is defined as a function $u \in L^2(\Omega)$ that fulfills the following conditions:

1. For $\alpha = \ell, \mathrm{g}$ the restriction of u on Ω^α has the following properties:
$$u_\alpha \in H^1(\Omega^\alpha) \qquad \text{and} \qquad u_\ell = H^{\Gamma_{\mathrm{LG}}} u_{\mathrm{g}} \text{ on } \Gamma_{\mathrm{LG}}.$$
This is equivalent to the requirement that
$$\widetilde{u} := \mathcal{H}u \qquad \text{with} \qquad \mathcal{H} := \begin{cases} 1 & \text{in} \quad \Omega^\ell \\ H^{\Gamma_{\mathrm{LG}}} & \text{in} \quad \Omega^{\mathrm{g}} \end{cases} \tag{2.2}$$
is an element of $H^1(\Omega)$ (since it is *continuous* across Γ_{LG}).
2. $\gamma_0(u)|_{\Gamma_{\mathrm{D}}} = u_{\mathrm{D}}$, where $\gamma_0 : H^1(\Omega^\ell \cup \Omega^{\mathrm{g}}) \to L^2(\partial\Omega)$ is the trace operator.
3. The following equation has to be satisfied for any smooth test function $\varphi \in C^\infty(\Omega)$:
$$\int_\Omega D\nabla u \cdot \nabla\varphi \, d\mathbf{x} - \int_{\Gamma_{\mathrm{D}}} D\nabla u\varphi \cdot \boldsymbol{\nu} \, d\sigma + \int_{\Gamma_{\mathrm{N}}} g_{\mathrm{N}}\varphi \, d\sigma = \int_\Omega f\varphi \, d\mathbf{x}, \tag{2.3}$$

The weak solution u is said to be k-regular, if additionally $u_\alpha \in H^k(\Omega^\alpha)$.

Note that (2.3) can be constructed from (2.1) by multiplying its first equation by φ and employing integration by parts. The integral at Γ_{LG} cancels due to the continuity of the flux. Thus, the jump condition is now hidden in the requirement that $\widetilde{u} \in H^1(\Omega)$. Moreover, this definition is not symmetric if $H^{\Gamma_{\mathrm{LG}}} \neq 1$, since u is supposed to be discontinuous across Γ_{LG}, while φ is supposed to be overall continuous. This imposes issues solely in the CG part and not in the DG part of the discretization, since its trial and test spaces do not comprise any continuity constraints.

3 The Enriched Galerkin Finite Element Method

3.1 Basic Definitions and Notations

In the following, $(\mathcal{T}_h)_{h>0}$ denotes a family of $\mathcal{T}_h := \mathcal{T}_h(\Omega) := \{\mathcal{K}_i : i = 1, \ldots, N_{\mathrm{el}}\}$ ($N_{\mathrm{el}} > 0$ is the amount of elements) being *d-dimensional non-overlapping partitions* of Ω (see [8, Def. 1.12]) that can be subdivided into $\mathcal{T}_h(\Omega^\ell)$ and $\mathcal{T}_h(\Omega^{\mathrm{g}})$ which are (families of) partitions of Ω^ℓ and Ω^{g}, respectively, and that is assumed to be *regular* (in the sense of [8, Def. 1.38]) and *geometrically conformal* (in the sense of [9, Def. 1.55]). For the sake of simplicity, we assume that $\mathcal{T}_h$ consists of simplices and/or quadrilaterals/hexahedrons. We denote by $\mathcal{F} = \mathcal{F}(\mathcal{T}_h)$ the set of *faces*, by $\mathcal{F}_{\mathrm{I}}$ the set of *interior faces* (that do not intersect with Γ_{LG}), by $\mathcal{F}_{\mathrm{E}}$ the set of *exterior faces*, and by $\mathcal{F}_\Gamma$ the set of faces that belong to Γ_{LG}. Henceforth, we assume that all $F \in \mathcal{F}_{\mathrm{E}}$ either are elements of $\mathcal{F}_{\mathrm{D}}$ (*Dirichlet boundary faces*) or of $\mathcal{F}_{\mathrm{N}}$ (*Neumann boundary faces*), and write $h_F = \operatorname{diam} F$ for the diameter of $F \in \mathcal{F}$, $\mathcal{F}_\mathcal{K}$ for the set of faces of $\mathcal{K} \in \mathcal{T}_h$, and $h_\mathcal{K}$ for the diameter of $\mathcal{K}$. Note that every face of the mesh is an element of one and only one of the following sets: $\mathcal{F}_{\mathrm{I}}, \mathcal{F}_\Gamma, \mathcal{F}_{\mathrm{D}}, \mathcal{F}_{\mathrm{N}}$. Beyond that, parameter h refers to the maximum diameter of an element of a mesh, i.e., $h = \max\{h_\mathcal{K} : \mathcal{K} \in \mathcal{T}_h\}$.

The *test* and *trial spaces* for our EG method utilize the *broken polynomial spaces of order at most m*

$$\mathbb{P}_m(\mathcal{T}_h) := \left\{ v \in L^2(\Omega) \,:\, v_{|\mathcal{K}} \text{ is a polynomial of degree at most } m, \forall \mathcal{K} \in \mathcal{T}_h \right\}$$

and are defined as

$$V_m^k := \left(\mathbb{P}_k(\mathcal{T}_h) \cap C(\Omega^\ell \cup \Omega^g) \right) + \mathbb{P}_m(\mathcal{T}_h)$$

for $-1 \leq m \leq k$, $k > 0$ (where $\mathbb{P}_{-1}(\mathcal{T}_h) = \{0\}$). Thus, obviously $\mathbb{P}_m(\mathcal{T}_h) \subset V_m^k \subset \mathbb{P}_k(\mathcal{T}_h)$. We additionally need a mapping combining the L^2 projection of degree at most m, Π_h^m, and interpolation of degree k denoted by I_h^k (and taking the values from the correct side if interpolation points on Γ_{LG} are considered), i.e

$$\boldsymbol{\pi} := \boldsymbol{\pi}_m^k : H^2(\Omega^\ell \cup \Omega^g) \to V_m^k \quad \text{and} \quad u \mapsto I_h^k u - \Pi_h^m I_h^k u + \Pi_h^m u. \tag{3.1}$$

Note that this map is not a projection since $V_m^k \not\subset H^2(\Omega^\ell \cup \Omega^g)$. However, using I_h^k instead of $\boldsymbol{\pi}$ would also satisfy all preconditions needed for the following analysis and therefore also is a proper choice, although it projects functions to a subspace of V_m^k only.

Remark 3.1 (Choice of projection (3.1) and prominent choices for m)

- If $m = -1$, the EG scheme becomes a classical CG discretization (since it reduces to the CG test and trial spaces where the DG and the CG bilinear forms are equivalent). In this case, the projection simplifies to the interpolation operator, which is the standard choice for CG. In addition, definition (3.1) also allows to replace I_h^k by other operators including the Clément or Scott–Zhang interpolations in order to define EG projections.
- If $m = k$, EG turns to the DG discretization. In this case, $\boldsymbol{\pi}$ is the standard L^2 projection, which also is the standard choice for DG.
- The most prominent choice is $m = 0$, which only adds the elementwise constants to the CG degrees of freedom. This choice still ensures the local conservation of mass with fewer number of degrees of freedom than DG. Here, $\boldsymbol{\pi}$ should be the sum of an overall continuous (elementwise polynomial of degree at most k) and an elementwise constant function. However, there is some freedom in the choice of representation, since the overall constant functions are included in both the overall continuous and the piecewise constant functions. In particular, the projection $\boldsymbol{\pi}$ does the following; the overall continuous function is defined by interpolation, while the piecewise constant function is defined as $\Pi_h^m(u - I_h^k u)$. Thus, the piecewise constant function represents the local mass error of the continuous part since L^2 projection to piecewise constants gives the elementwise mean values which directly represent the mass.
- Analogously, to the above case, if $0 \leq m < k$, the projection $\boldsymbol{\pi}$ can be split into a continuous part and an elementwise error part of the moments up to order m.

For an element-wise defined scalar function w and an element-wise vector function $\mathbf{v}$, we define the average $\{\!\{\cdot\}\!\}$ and the jump $[\![\cdot]\!]$ on $\partial\mathcal{K}_i \cap \partial\mathcal{K}_j$ for neighboring mesh elements $\mathcal{K}_i, \mathcal{K}_j \in \mathcal{T}_h$, $\mathcal{K}_i \neq \mathcal{K}_j$ in the following way:

$$[\![w]\!] := w_{|\mathcal{K}_i} \boldsymbol{\nu}_{\mathcal{K}_i} + w_{|\mathcal{K}_j} \boldsymbol{\nu}_{\mathcal{K}_j} \quad \text{and} \quad \{\!\{\mathbf{v}\}\!\} := \frac{1}{2}\mathbf{v}_{|\mathcal{K}_i} + \frac{1}{2}\mathbf{v}_{|\mathcal{K}_j},$$

where $\boldsymbol{\nu}_{\mathcal{K}}$ is defined as the outward unit normal with respect to $\mathcal{K}$. Note, that a jump in a scalar variable is a vector, and that jump and average on $F \in \mathcal{F}_{\mathrm{E}}$ with $F \subset \partial\mathcal{K}$ are defined as

$$[\![w]\!] := w_{|\mathcal{K}} \boldsymbol{\nu}_{\mathcal{K}} \quad \text{and} \quad \{\!\{\mathbf{v}\}\!\} := \mathbf{v}_{|\mathcal{K}}.$$

3.2 Spatial Discretization

Next, we formulate the discrete problem with the above definitions. Here, we have to be careful defining numerical fluxes across Γ_{LG} since they have to be both locally mass conservative and stable. This is done in the following way for every $\mathcal{K} \in \mathcal{T}_h(\Omega)$ and every test function ψ. Note that $u_h, \psi \in V_m^k$. Since the equation is linear, we can rescale the equation by $H^{\Gamma_{\mathrm{LG}}}$ in Ω^{g} and by 1 in Ω^{ℓ}. This yields local bilinear and linear forms as:

$$
\begin{aligned}
a_{\mathrm{loc}}(u_h, \psi) &:= \int_{\mathcal{K}} D\nabla u_h \cdot \mathcal{H}\nabla\psi \, d\mathbf{x} + \sum_{F \in \mathcal{F}_{\mathcal{K}}} \int_F \widehat{\mathcal{H}\mathcal{Q}_F^{\mathcal{K}}} \, d\sigma, \\
b_{\mathrm{loc}}(\psi) &:= \int_{\mathcal{K}} f\mathcal{H}\psi \, d\mathbf{x} + \int_{\partial\mathcal{K}\cap\Gamma_{\mathrm{D}}} \left[\mu\mathcal{H}D\nabla\psi u_D \cdot \nu_{\mathcal{K}} + \frac{\mathcal{H}^2\eta}{h_F} u_{\mathrm{D}} \psi \right] d\sigma \\
&\quad - \int_{\partial\mathcal{K}\cap\Gamma_{\mathrm{N}}} \mathcal{H} g_{\mathrm{N}} \psi \, d\sigma,
\end{aligned}
$$

where $\mathcal{H}$ is defined as in (2.2) and the inter-element flux $\widehat{\mathcal{H}\mathcal{Q}_F^{\mathcal{K}}}$ is defined as

$$
\widehat{\mathcal{H}\mathcal{Q}_F^{\mathcal{K}}} := \begin{cases} \mu\mathcal{H}D\nabla\psi u_h \cdot \boldsymbol{\nu}_{\mathcal{K}} - \mathcal{H}D\nabla u_h\psi \cdot \boldsymbol{\nu}_{\mathcal{K}} + \mathcal{H}^2 \frac{\eta}{h_F} u_h\psi & \text{on } \Gamma_{\mathrm{D}}, \\ 0 & \text{on } \Gamma_{\mathrm{N}}, \\ \mu\{\!\{D\nabla\psi\}\!\}[\![\mathcal{H}u_h]\!] \cdot \boldsymbol{\nu}_{\mathcal{K}} - \{\!\{D\nabla u_h\}\!\}\mathcal{H}\psi \cdot \boldsymbol{\nu}_{\mathcal{K}} + \frac{\eta}{h_F}[\![\mathcal{H}u_h]\!]\mathcal{H}\psi \cdot \boldsymbol{\nu}_{\mathcal{K}} & \text{otherwise.} \end{cases}
$$

An alternate, equivalent way of defining $\widehat{\mathcal{H}\mathcal{Q}_F^{\mathcal{K}}}$ is as

$$
\widehat{\mathcal{H}\mathcal{Q}_F^{\mathcal{K}}} := \begin{cases} \mu\mathcal{H}D\nabla\psi u_h \cdot \boldsymbol{\nu}_{\mathcal{K}} - \mathcal{H}D\nabla u_h\psi \cdot \boldsymbol{\nu}_{\mathcal{K}} + \mathcal{H}^2 \frac{\eta}{h_F} u_h\psi & \text{on } \Gamma_{\mathrm{D}}, \\ 0 & \text{on } \Gamma_{\mathrm{N}}, \\ \frac{\mu}{2}[\![\mathcal{H}u_h]\!] \cdot D\nabla\psi - \{\!\{D\nabla u_h\}\!\}\mathcal{H}\psi \cdot \boldsymbol{\nu}_{\mathcal{K}} + \frac{\eta}{h_F}[\![\mathcal{H}u_h]\!]\mathcal{H}\psi \cdot \boldsymbol{\nu}_{\mathcal{K}} & \text{otherwise.} \end{cases}
$$

Note that we penalize the jump in $\mathcal{H}u_h = \widetilde{u}_h$ but not the jump in u_h. That is due to the fact that $\widetilde{u}_h$ is supposed to be the overall continuous function. Alternatively, one could also penalize the jump in u_h on all faces, but those that coincide with Γ_{LG}, and the jump in $\widetilde{u}_h$ on those faces that coincide with Γ_{LG}. However, the latter is not considered here. Moreover, our local rescaling leads to the fact that $\widetilde{\psi} = \mathcal{H}\psi$ (and not ψ) plays the role of the overall continuous test function.

Summation over all elements (in both cases) leads to the global form of the equation

$$
a_h(u_h, \psi) = b_h(\psi), \tag{3.2a}
$$

where the bilinear form a_h is defined as

$$
\begin{aligned}
a_h(u_h, \psi) &:= \sum_{\mathcal{K}\in\mathcal{T}_h} \int_{\mathcal{K}} D\nabla u_h \cdot \mathcal{H}\nabla\psi \, d\mathbf{x} \\
&\quad + \sum_{F \in \mathcal{F}_{\mathrm{I}}\cup\mathcal{F}_{\mathrm{D}}\cup\mathcal{F}_{\Gamma}} \int_F \left[\mu\{\!\{D\nabla\psi\}\!\} \cdot [\![\mathcal{H}u_h]\!] - \{\!\{D\nabla u_h\}\!\} \cdot [\![\mathcal{H}\psi]\!] + \frac{\eta}{h_F}[\![\mathcal{H}u_h]\!] \cdot [\![\mathcal{H}\psi]\!] \right] d\sigma,
\end{aligned} \tag{3.2b}
$$

and the linear form b_h is

$$
b_h(\psi) := \int_{\Omega} \mathcal{H} f\psi \, d\mathbf{x} + \int_{\Gamma_{\mathrm{D}}} \left[\mu\mathcal{H}D\nabla\psi u_D \cdot \nu_{\mathcal{K}} + \frac{\mathcal{H}^2\eta}{h_F} u_{\mathrm{D}}\psi \right] d\sigma - \int_{\Gamma_{\mathrm{N}}} \mathcal{H} g_{\mathrm{N}}\psi \, d\sigma. \tag{3.2c}
$$

Both forms depend on the choice of the symmetrization parameter μ and the penalty parameter η. Note that $\mu = 1$ corresponds to the Non-Symmetric Interior Penalty (NIP-DG), $\mu = 0$ to the Incomplete Interior Penalty (IIP-DG), and $\mu = -1$ to the Symmetric Interior Penalty (SIP-DG) discontinuous Galerkin methods if $k = m$. In that sense, they can be generalized to their enriched Galerkin versions NIP-EG, IIP-EG, and SIP-EG, respectively. The penalty parameter η needs to be chosen appropriately to ensure the stability of the method.

The implementation of DG is straightforward with this definition, whereas a correct implementation of the equation with the CG method uses the H^1 regularity of $\widetilde{u}$. Thus, we consider the bilinear form $\widetilde{a}_h$ and linear form $\widetilde{b}_h$ to approximate $\widetilde{u}$, i.e., in terms of $\widetilde{u}_h$, $\widetilde{\psi}$:

$$\widetilde{a}_h(\widetilde{u}_h, \widetilde{\psi}) = \widetilde{b}_h(\widetilde{\psi}), \tag{3.3a}$$

$$\begin{aligned}\widetilde{a}_h(\widetilde{u}_h, \widetilde{\psi}) = &\sum_{\mathcal{K}\in\mathcal{T}_h} \int_{\mathcal{K}} \frac{1}{\mathcal{H}} D\nabla\widetilde{u}_h \cdot \nabla\widetilde{\psi}\, d\mathbf{x} \\ &+ \sum_{F\in\mathcal{F}_\mathrm{I}\cup\mathcal{F}_\mathrm{D}\cup\mathcal{F}_\Gamma} \int_F \left[\mu \{\!\{\tfrac{1}{\mathcal{H}} D\nabla\widetilde{\psi}\}\!\} \cdot [\![\widetilde{u}_h]\!] - \{\!\{\tfrac{1}{\mathcal{H}} D\nabla\widetilde{u}_h\}\!\} \cdot [\![\widetilde{\psi}]\!] + \frac{\eta}{h_F} [\![\widetilde{u}_h]\!] \cdot [\![\widetilde{\psi}]\!]\right] d\sigma,\end{aligned} \tag{3.3b}$$

$$\widetilde{b}_h(\widetilde{\psi}) = \int_\Omega f\widetilde{\psi}\, d\mathbf{x} + \int_{\Gamma_\mathrm{D}} \left[\mu D\nabla\widetilde{\psi} u_D \cdot \nu_\mathcal{K} + \frac{\eta\mathcal{H}}{h_F} u_\mathrm{D}\widetilde{\psi}\right] d\sigma - \int_{\Gamma_\mathrm{N}} g_\mathrm{N}\widetilde{\psi}\, d\sigma. \tag{3.3c}$$

Note that this actually does not change the bilinear forms at all, but changes the way of interpretation. Instead of solving the equations for u using test and trial functions ψ, u_h, we solve for $\widetilde{u}$ with test and trial functions $\widetilde{\psi}$, $\widetilde{u}_h$. Thus, if $\widetilde{u}_h$ is calculated, one can get u_h by a simple post-processing step via $u_h = \widetilde{u}_h/\mathcal{H}$.

Remark 3.2 **(Difference of formulations (3.2) and (3.3))** Since both schemes are equivalent, they can both be considered as symmetric, antisymmetric, etc. if the corresponding other one is symmetric, antisymmetric, etc., respectively. The important difference is in the choice of the test and trial spaces. For (3.2), the test and trial spaces for u_h, ψ are $V_m^k = \left(\mathbb{P}_k(\mathcal{T}_h) \cap C(\Omega^\ell \cup \Omega^\mathrm{g})\right) + \mathbb{P}_m(\mathcal{T}_h)$, while $\widetilde{u}_h, \widetilde{\psi}$ in (3.3) are continuous across Γ_LG. Thus, $\widetilde{a}_h$ and $\widetilde{b}_h$ can act on $\widetilde{V}_m^k := \left(\mathbb{P}_k(\mathcal{T}_h) \cap C(\overline{\Omega})\right) + \mathbb{P}_m(\mathcal{T}_h)$ if the continuity constraint is enforced strongly for the overall continuous test and trial functions. This is more in line with the standard finite element spaces (but does not affect any analysis arguments that are to follow). Thus, the standard finite element method does not need to be changed at all to approximate the solution of our specific problem (with the jump condition—only D and u_D need to be rescaled and a postprocessing step needs to be done). This is one major benefit of the proposed scheme and can directly be utilized for the EG scheme. This approach allows to calculate a solution with jump conditions using any finite element toolbox and exploiting its specific advantages. In particular, we present the standard analysis tools for the specific methods (CG, DG, EG) and combine them to a uniform analysis.

This gives an enormous amount of freedom for implementation if the DG scheme is considered, i.e., $k = m$: One could use both presented schemes, where the first (in terms of u_h and ψ) is to be preferred — due to the fact that no post-processing is necessary.

If one uses a CG discretization (with $m = -1$), the second variant is recommended since there is no need to adapt your CG code (except for the local rescaling and the post-processing). It contains all the advantages of a CG discretization and the forms even simplify to

$$\widetilde{a}_h(\widetilde{u}_h, \widetilde{\psi}) = \int_\Omega \frac{1}{\mathcal{H}} D\nabla\widetilde{u}_h \cdot \nabla\widetilde{\psi}\, d\mathbf{x}, \qquad \widetilde{b}_h(\widetilde{\psi}) = \int_\Omega f\widetilde{\psi}\, d\mathbf{x} - \int_{\Gamma_\mathrm{N}} g_\mathrm{N}\widetilde{\psi}\, d\sigma,$$

if the homogeneous Dirichlet boundary values are incorporated in the test and trial spaces. In this case, a post-processing step (dividing $\mathcal{H}$ pointwise) is needed to obtain u_h if $\widetilde{u}_h$ is computed. If one uses the EG scheme with $0 < m < k$, we highly recommend to use (3.3) for implementation and do the post-processing.

Since switching between the equivalent formulations (3.2) and (3.3) is tedious and in general (3.3) is to be preferred for implementation, we will focus on formulation (3.3) for the following analysis and implementation. Finally, one easily verifies that

Corollary 3.3 *The numerical discretization (3.3) is consistent with respect to Definition 2.2 that is, the above equations hold for $\widetilde{u} = \mathcal{H}u$ and u being the 2-regular, weak solution of (2.1).*

4 Stability and Error Analysis

In the following, we utilize $V_m^k \subset \mathbb{P}_k(\mathcal{T}_h)$ to extend the standard DG results to our EG scheme.

4.1 A Collection of Auxiliary Definitions and Results

We give a brief overview of auxiliary definitions and results that are needed for the following analysis. At first, we define the operator $\widetilde{\cdot}$ like in (2.2), i.e. for any function ξ on Ω

$$\widetilde{\xi} := \mathcal{H}\xi := \begin{cases} \xi & \text{in} \quad \Omega^\ell, \\ H^{\Gamma_{\mathrm{LG}}}\xi & \text{in} \quad \Omega^{\mathrm{g}}. \end{cases}$$

In addition, we define norms on the *broken Sobolev space*

$$H^2(\mathcal{T}_h) := \{v \in L^2(\Omega) \,:\, v \in H^2(\mathcal{K}) \text{ for all } \mathcal{K} \in \mathcal{T}_h\}$$

with *induced broken Sobolev norm* $\|\cdot\|_{H^2(\mathcal{T}_h)}$ via

$$\begin{aligned} \|v\|_{H^r(\mathcal{T}_h)}^2 &:= \|v\|_{L^2(\Omega)}^2 + \sum_{i=1}^{r} |v|_{H^i(\mathcal{T}_h)}^2, \\ |v|_{H^i(\mathcal{T}_h)}^2 &:= \sum_{\mathcal{K}\in\mathcal{T}_h} |v|_{H^i(\mathcal{K})}^2, \\ \|v\|_{\mathrm{IP}}^2 &:= \sum_{\mathcal{K}\in\mathcal{T}_h} \|\sqrt{\tfrac{1}{\mathcal{H}} D}\nabla v\|_{L^2(\mathcal{K})}^2 + \sum_{F\in\mathcal{F}\setminus\mathcal{F}_{\mathrm{N}}} \frac{\eta}{h_F} \|[\![v]\!]\|_{L^2(F)}^2, \\ \|v\|_{\mathrm{IP}*}^2 &:= \|v\|_{\mathrm{IP}}^2 + \sum_{F\in\mathcal{F}\setminus\mathcal{F}_{\mathrm{N}}} \frac{h_F}{\eta} \|\{\!\{\tfrac{1}{\mathcal{H}} D\nabla v\}\!\}\|_{L^2(F)}^2, \end{aligned}$$

with $r \in \mathbb{N}$ and $\eta > 0$. Note that $H^2(\Omega^\ell \cup \Omega^{\mathrm{g}}) \subset H^2(\mathcal{T}_h)$ and $V_m^k \subset H^2(\mathcal{T}_h)$, while $V_m^k \not\subset H^2(\Omega^\ell \cup \Omega^{\mathrm{g}})$. Similar norms can be found in [8], where the η has been extracted, and neither $\mathcal{H}$ nor D are present.

Lemma 4.1 (Discrete trace inequality) *Let $(\mathcal{T}_h)_{h>0}$ be as in Sect. 3.1. Then, there is a constant C_{tr} such that for all $h > 0$, all $p \in \mathbb{P}_k(\mathcal{T}_h)$, and all $\mathcal{K} \in \mathcal{T}_h$,*

$$h_{\mathcal{K}}^{1/2} \sum_{F\in\mathcal{F}_{\mathcal{K}}} \|p\|_{L^2(F)} \le C_{\mathrm{tr}} \|p\|_{L^2(\mathcal{K})} \text{ and } h_{\mathcal{K}}^{1/2} \sum_{F\in\mathcal{F}_{\mathcal{K}}} \|\nabla p\|_{L^2(F)} \le C_{\mathrm{tr}} \|\nabla p\|_{L^2(\mathcal{K})}.$$

Proof Follows directly from [8, Lemma 1.46]. □

Lemma 4.2 (Continuous trace inequality) *Let $(\mathcal{T}_h)_{h>0}$ be as in Sect. 3.1. Then, there is a constant $C_{\text{trace}} > 0$ such that for all $h > 0$, all $v \in H^1(\mathcal{T}_h)$, all $\mathcal{K} \in \mathcal{T}_h$, and all $F \in \mathcal{F}_\mathcal{K}$*

$$\|v\|^2_{L^2(F)} \leq C_{\text{trace}} \left(2\|\nabla v\|_{L^2(\mathcal{K})} + dh_\mathcal{K}^{-1}\|v\|_{L^2(\mathcal{K})}\right) \|v\|_{L^2(\mathcal{K})}.$$

Proof See [8, Lemma 1.49]. □

Since we have a regular and simplicial/hexahedral triangulation, we have a constant $\rho > 0$ with $h_F \geq \rho h_\mathcal{K}$ if $\mathcal{K}$ is adjacent to F. Thus, Lemma 4.2 and Young's inequality imply that there is a constant C (independent of h) such that

$$\|v\|^2_{\text{IP}*} \leq C \sum_{\mathcal{K}\in\mathcal{T}_h} \left[h_\mathcal{K}^{-2}\|v\|^2_{L^2(\mathcal{K})} + |v|^2_{H^1(\mathcal{K})} + h^2_\mathcal{K}|v|^2_{H^2(\mathcal{K})}\right] \qquad \forall v \in H^2(\mathcal{T}_h). \tag{4.1}$$

We also obtain the following result:

Lemma 4.3 *There is a constant $C_{\text{Poin}} > 0$ independent of $h > 0$ such that for all $v_h \in V_m^k$*

$$\|v_h\|_{L^2(\Omega)} \leq C_{\text{Poin}}\|v_h\|_{\text{IP}}.$$

Proof See [8, pp. 190–192]. □

4.2 Coercivity and Boundedness of Forms

In this section, we start from the following lemma:

Lemma 4.4 *The linear form $\widetilde{b}_h$ and bilinear form $\widetilde{a}_h$ are bounded on V_m^k in terms of $\|\cdot\|_{\text{IP}}$. The bilinear form $\widetilde{a}_h$ is uniformly coercive in $\|\cdot\|_{\text{IP}}$ with parameter $\widetilde{\alpha}$ independent of h provided that*

$$\eta > \tfrac{1}{4}|(1-\mu)|^2 C_{\text{tr}}^2 C_D^3 \underline{\mathcal{H}}^2 \overline{\mathcal{H}} N_\partial \tag{4.2}$$

with $\underline{\mathcal{H}} = \sup\{1/\mathcal{H}(\mathbf{x}) : \mathbf{x} \in \Omega\}$, $\overline{\mathcal{H}} = \sup\{\mathcal{H}(\mathbf{x}) : \mathbf{x} \in \Omega\}$, and N_∂ being the maximum number of faces of an element.

In the case of simplicial meshes, $N_\partial = d + 1$. Lemma 4.4 implies uniform stability for the NIP-DG(EG) method, where $\mu = 1$, if $\eta > 0$, and directly ensures that the Lax–Milgram Lemma can be applied guaranteeing that there is a unique solution of (3.3).

Proof For the coercivity of $\widetilde{a}_h$ consider $v_h \in V_m^k$ and observe that

$$\widetilde{a}_h(v_h, v_h) = \|v_h\|^2_{\text{IP}} \underbrace{-(1-\mu) \sum_{F\in\mathcal{F}\setminus\mathcal{F}_\text{N}} \int_F \{\!\!\{ \tfrac{1}{\mathcal{H}} D\nabla v_h \}\!\!\} \cdot [\![v_h]\!] \, d\sigma}_{=:(\bigstar)}.$$

Thus, it is sufficient to bound the absolute value of $(\bigstar)$ by means of $\|v_h\|^2_{\text{IP}}$ to ensure the coercivity. This can be done by utilizing that D is bounded and symmetric positive definite, Lemma 4.1, and Hölder's and Young's inequalities as

$$|(\bigstar)| \leq |(1-\mu)| \sum_{F\in\mathcal{F}\setminus\mathcal{F}_\text{N}} C_D \underline{\mathcal{H}} \|\{\!\!\{\nabla v_h\}\!\!\}\|_{L^2(F)} \|[\![v_h]\!]\|_{L^2(F)}$$

$$\leq |(1-\mu)| \sum_{F\in\mathcal{F}\setminus\mathcal{F}_N} C_D \underline{\mathcal{H}} C_{\mathrm{tr}} \|\nabla v_h\|_{L^2(\mathcal{K}_F)} h_F^{-1/2} \|[\![v_h]\!]\|_{L^2(F)}$$

$$\leq \delta \sum_{F\in\mathcal{F}\setminus\mathcal{F}_N} \|\sqrt{\tfrac{1}{\mathcal{H}} D}\nabla v_h\|^2_{L^2(\mathcal{K}_F)} + \sum_{F\in\mathcal{F}\setminus\mathcal{F}_N} \frac{|(1-\mu)|^2 C_{\mathrm{tr}}^2 C_D^2 \underline{\mathcal{H}}^2 \overline{\mathcal{H}}}{4\delta C_D^{-1} h_F} \|[\![v_h]\!]\|^2_{L^2(F)},$$

where $\mathcal{K}_F$ denotes (the union of) the element(s) with face F and $0 < \delta < 1/N_\partial$. Boundedness is also obvious since all bilinear and linear forms on finite dimensional spaces are bounded. □

Then, we obtain the following result:

Lemma 4.5 *For $w_h \in H^2(\mathcal{T}_h)$ and $v_h \in V_m^k$ there is a constant $\widetilde{M}$ independent of h such that*

$$\widetilde{a}_h(w_h, v_h) \leq \widetilde{M} \|w_h\|_{\mathrm{IP}*} \|v_h\|_{\mathrm{IP}}.$$

Proof Using Lemma 4.1 for v_h and exploiting the definitions of $\|\cdot\|_{\mathrm{IP}*}$ for w_h immediately gives the result using the techniques of the proof of Lemma 4.4 and the Cauchy–Schwarz inequality. □

4.3 Convergence Order Estimates

Due to Corollary 3.3 and Lemmas 4.3, 4.4, and 4.5, we have the following result for $v_h \in V_m^k$

$$C_{\mathrm{Poin}}^{-1} \widetilde{\alpha} \|\widetilde{u}_h - v_h\|_{L^2(\Omega)} \leq \widetilde{\alpha} \|\widetilde{u}_h - v_h\|_{\mathrm{IP}} \leq \sup_{w_h \in V_m^k \setminus \{0\}} \frac{\widetilde{a}_h(\widetilde{u}_h - v_h, w_h)}{\|w_h\|_{\mathrm{IP}}}$$

$$\leq \sup_{w_h \in V_m^k \setminus \{0\}} \frac{\widetilde{a}_h(\widetilde{u} - v_h, w_h)}{\|w_h\|_{\mathrm{IP}}} \leq \widetilde{M} \|\widetilde{u} - v_h\|_{\mathrm{IP}*} \tag{4.3}$$

if u is 2-regular. By setting $v_h = \boldsymbol{\pi}\widetilde{u}$, it is required to show that

$$\|\widetilde{u} - \boldsymbol{\pi}\widetilde{u}\|_{\mathrm{IP}*} \leq C h^k |u|_{H^{k+1}(\Omega^\ell \cup \Omega^g)}$$

for the convergence of $\widetilde{u} - \boldsymbol{\pi}\widetilde{u}$ with order at most k in the energy, the L^2, and the broken H^1 norms. Thus, we start from the following lemma:

Lemma 4.6 *For a mesh sequence as in Sect. 3.1 and with $\boldsymbol{\pi}$ as defined in (3.1), we have*

$$\|\widetilde{u} - \boldsymbol{\pi}\widetilde{u}\|_{\mathrm{IP}*} \leq C h^k |u|_{H^{k+1}(\Omega^\ell \cup \Omega^g)}$$

if u is $(k+1)$-regular. □

Proof The result can be obtained by using (4.1) and the standard scaling argument in combination with the Bramble–Hilbert Lemma (cf. [15, Sect. 3.4.1] with $\boldsymbol{\pi}$ instead of the interpolation). □

Then the above Lemma directly implies a convergence result:

Theorem 4.7 *Under the preconditions of Sect. 3.1 and 2, we have*

$$\|\widetilde{u} - \widetilde{u}_h\|_{H^1(\mathcal{T}_h)} \leq C h^k |u|_{H^{k+1}(\Omega^\ell \cup \Omega^g)}.$$

if u is $(k+1)$-regular.

Proof We have

$$\begin{aligned}\|\widetilde{u}-\widetilde{u}_h\|_{L^2(\Omega)} &\leq \|\widetilde{u}-\boldsymbol{\pi}\widetilde{u}\|_{L^2(\Omega)} + \|\boldsymbol{\pi}\widetilde{u}-\widetilde{u}_h\|_{L^2(\Omega)} \\ &\leq Ch^{k+1}|u|_{H^{k+1}(\Omega^\ell\cup\Omega^{\mathrm{g}})} + Ch^{k}|u|_{H^{k+1}(\Omega^\ell\cup\Omega^{\mathrm{g}})},\end{aligned}$$

where the first summand is bounded by direct application of the standard scaling argument and the second one is due to (4.3) and Lemma 4.6. Analogously (since the broken H^1 semi-norm is incorporated in $\|\cdot\|_{\mathrm{IP}}$), one obtains the result for $\|\cdot\|_{H^1(\mathcal{T}_h)}$. □

In order to show the optimal order of convergence for SIP-EG, i.e. the case with $\mu=-1$, we note that $\widetilde{a}_h$ is symmetric and consistent. By assuming an adapted version of elliptic regularity, we want that $\varphi\in H^1(\Omega^\ell\cup\Omega^{\mathrm{g}})$ with $\widetilde{\varphi}\in H^1(\Omega)$ and $\gamma_0(\varphi)|_{\Gamma_{\mathrm{D}}}=0$ being the solution of

$$\int_\Omega D\nabla\varphi\nabla\psi\,d\mathbf{x} - \int_{\Gamma_{\mathrm{D}}} D\nabla\varphi\psi\cdot\boldsymbol{\nu}\,d\sigma = \int_\Omega \lambda\psi \qquad \forall\psi\in H^1(\Omega) \tag{4.4}$$

is in $H^2(\Omega^\ell\cup\Omega^{\mathrm{g}})$ for all $\lambda\in L^2(\Omega)$, and that we have $|\varphi|_{H^2(\Omega^\ell\cup\Omega^{\mathrm{g}})}\leq C\|\lambda\|_{L^2(\Omega)}$. This is realistic since our assumption formally is weaker than standard H^2 regularity, and it fits perfectly to our problem. An investigation of the elliptic regularity constants for similar equations can be found in [7,10]. Then, we obtain the following theorem:

Theorem 4.8 *If $\mu=-1$ and the problem has the aforementioned version of elliptic regularity, we have under the preconditions of Theorem 4.7 that*

$$\|\widetilde{u}-\widetilde{u}_h\|_{L^2(\Omega)}\leq Ch^{k+1}|\widetilde{u}|_{k+1}$$

if u is $(k+1)$-regular.

Proof Setting $\lambda=\widetilde{u}-\widetilde{u}_h$ and testing (4.4) with $\widetilde{u}-\widetilde{u}_h$ yields

$$\begin{aligned}\|\widetilde{u}-\widetilde{u}_h\|^2_{L^2(\Omega)} &= \widetilde{a}_h(\widetilde{\varphi},\widetilde{u}-\widetilde{u}_h) = \widetilde{a}_h(\widetilde{u}-\widetilde{u}_h,\widetilde{\varphi}) = \widetilde{a}_h(\widetilde{u}-\widetilde{u}_h,\widetilde{\varphi}-\boldsymbol{\pi}^1_r\widetilde{\varphi}) \\ &\leq C\|\widetilde{u}-\widetilde{u}_h\|_{\mathrm{IP}*}\|\widetilde{\varphi}-\boldsymbol{\pi}^1_r\widetilde{\varphi}\|_{\mathrm{IP}*},\end{aligned}$$

where $r=\min\{1,m\}$. The first equality follows from consistency of the method, the second equality holds due to symmetry, and the third equality is error orthogonality of $\widetilde{a}_h$. The inequality can be obtained analogously to Lemma 4.5. The fact that

$$\|\widetilde{\varphi}-\boldsymbol{\pi}^1_{-1}\widetilde{\varphi}\|_{\mathrm{IP}*}\leq Ch|\widetilde{\varphi}|_{H^2(\Omega^\ell\cup\Omega^{\mathrm{g}})}\leq Ch\|\widetilde{u}-\widetilde{u}_h\|_{L^2(\Omega)}$$

gives the result together with the uniform equivalence of $\|\cdot\|_{\mathrm{IP}}$ and $\|\cdot\|_{\mathrm{IP}*}$ on V_m^k (cf. [8, Lem. 4.20]) and Lemma 4.6 after dividing by $\|\widetilde{u}-\widetilde{u}_h\|_{L^2(\Omega)}$ on both sides. □

Remark 4.9 Note that the whole analysis of EG turns out to be independent of the choice for the polynomial order m. Thus, the value of m does not effect the results for the optimal error convergence rate. Corresponding numerical experiments are presented in Sect. 6. Consequently, in practice, it generally makes sense to choose m for EG as small as necessary to ensure the desired properties.

5 Parabolic Problem

The parabolic problem is similar to the aforementioned elliptic problem (2.1) but involves the time derivative term as defined in the following

$$\begin{cases} \partial_t u - \nabla \cdot (D\nabla u) = f & \text{in} \quad (0,T) \times \left(\Omega^\ell \cup \Omega^{\mathrm{g}}\right), \\ u_\ell / u_{\mathrm{g}} = H^{\Gamma_{\mathrm{LG}}} & \text{on} \quad (0,T) \times \Gamma_{\mathrm{LG}}, \\ D_\ell \nabla u_\ell \cdot \boldsymbol{\nu}_\ell + D_{\mathrm{g}} \nabla u_{\mathrm{g}} \cdot \boldsymbol{\nu}_{\mathrm{g}} = 0 & \text{on} \quad (0,T) \times \Gamma_{\mathrm{LG}}, \\ -D\nabla u \cdot \boldsymbol{\nu} = g_{\mathrm{N}} & \text{on} \quad (0,T) \times \Gamma_{\mathrm{N}}, \\ u = u_{\mathrm{D}} & \text{on} \quad (0,T) \times \Gamma_{\mathrm{D}}, \\ u(0,\mathbf{x}) = u_0(\mathbf{x}) & \text{in} \quad \Omega^\ell \cup \Omega^{\mathrm{g}}, \end{cases} \tag{5.1}$$

for a given $D \in L^\infty(0,T; W^{1,\infty}(\Omega^\ell \cup \Omega^{\mathrm{g}})^{d,d})$ which is uniformly symmetric positive definite (also in time), $H^{\Gamma_{\mathrm{LG}}} \in \mathbb{R}^+$, $f \in L^2((0,T) \times \Omega)$, and $u_{\mathrm{D}}, g_{\mathrm{N}} \in L^2(0,T; H^1(\Omega^\ell \cup \Omega^{\mathrm{g}}))$ sufficing the conditions at Γ_{LG} as $u_0 \in H^2(\Omega^\ell \cup \Omega^{\mathrm{g}})$ does.

We first define the weak solution and regularity for the above problem by

Definition 5.1 (*Weak solution and regularity*) A weak solution of (5.1) is a function $u \in H^1(0,T; L^2(\Omega))$ that fulfills item 1 and item 2 of Definition 2.2 for almost every (a.e.) $t \in (0,T)$. The item 3 in Definition 2.2 is replaced by $u(0) = u_0$ and the condition that for a.e. $t \in (0,T)$ and arbitrary $\varphi \in C^\infty(\Omega)$

$$\int_\Omega \partial_t u \varphi \, d\mathbf{x} + \int_\Omega D\nabla u \cdot \nabla \varphi \, d\mathbf{x} - \int_{\Gamma_{\mathrm{D}}} D\nabla u \varphi \cdot \boldsymbol{\nu} \, d\sigma + \int_{\Gamma_{\mathrm{N}}} g_{\mathrm{N}} \varphi \, d\sigma = \int_\Omega f \varphi \, d\mathbf{x}$$

The weak solution u is said to be k-regular, if additionally $u_\alpha \in L^2(0,T; H^k(\Omega^\alpha))$.

Then, the discrete version of this equation is to find $u_h \in H^1(0,T; V_m^k)$ such that for a.e. $t \in (0,T)$

$$\int_\Omega \left(\partial_t \frac{1}{\mathcal{H}} \widetilde{u}_h \right) \widetilde{\psi} \, d\mathbf{x} + \widetilde{a}_h(\widetilde{u}_h, \widetilde{\psi}) = \widetilde{b}_h(\widetilde{\psi}) \qquad \forall \widetilde{\psi} \in V_m^k,$$

where the bilinear and linear forms are time-dependent and the initial $u_h(0)$ is a suitable approximate of u_0. The specific choice of $u_h(0)$ will influence our error analysis and will therefore be presented at the beginning of Sects. 5.1 and 5.2, respectively. Moreover, by assuming the elliptic regularity, Theorems 5.3 and 5.5 can be improved with respect to the $L^\infty(L^2)$ errors if $\mu = -1$ (symmetry) by utilizing the standard duality argument (cf. the proof of Theorem 4.8 or [8, Sect. 4.7.5] for fully discrete arguments and more details).

5.1 Standard Semi-discrete Arguments

With the above definitions, the results of Sects. 4.1 and 4.2 for elliptic problem still hold uniformly in time. Thus, $\widetilde{u}_h(0) = \boldsymbol{\pi} \widetilde{u}_0$ [with $\boldsymbol{\pi}$ as defined in (3.1)] seems an intuitive choice, and we can conduct a semi-discrete error analysis using

$$\widetilde{e}_u := \widetilde{u}_h - \boldsymbol{\pi} \widetilde{u} \qquad \text{and} \qquad \widetilde{\theta}_u := \boldsymbol{\pi} \widetilde{u} - \widetilde{u}.$$

We start from the following lemma:

Lemma 5.2 *For almost every $t \in (0,T)$, we have*

$$\|\widetilde{e}_u(t)\|_{L^2(\Omega)}^2 + \int_0^t \|\widetilde{e}_u(s)\|_{\mathrm{IP}}^2 \, ds \le C \int_0^t \left[\|\partial_t \widetilde{\theta}_u(s)\|_{L^2(\Omega)}^2 + \|\widetilde{\theta}_u(s)\|_{\mathrm{IP}*}^2 \right] ds$$

Proof Due to the consistency of the method, the error equation

$$\int_\Omega \frac{1}{\mathcal{H}} \partial_t (\widetilde{e}_u + \widetilde{\theta}_u) \widetilde{e}_u \, d\mathbf{x} + \widetilde{a}_h(\widetilde{e}_u + \widetilde{\theta}_u, \widetilde{e}_u) = 0$$

holds for a.e. $t \in (0, T)$. Simple algebraic manipulations give us that

$$\begin{aligned} \frac{1}{2} \partial_t \| \sqrt{\tfrac{1}{\mathcal{H}}} \widetilde{e}_u \|^2_{L^2(\Omega)} + \widetilde{a}_h(\widetilde{e}_u, \widetilde{e}_u) &= - \int_\Omega \tfrac{1}{\mathcal{H}} \partial_t \widetilde{\theta}_u \widetilde{e}_u \, d\mathbf{x} - \widetilde{a}_h(\widetilde{\theta}_u, \widetilde{e}_u) \\ &\leq \frac{\epsilon}{2} \| \widetilde{e}_u \|^2_{L^2(\Omega)} + \frac{C}{2\epsilon} \| \partial_t \widetilde{\theta}_u \|^2_{L^2(\Omega)} + \frac{\epsilon}{2} \| \widetilde{e}_u \|^2_{\mathrm{IP}} + \frac{\widetilde{M}^2}{2\epsilon} \| \widetilde{\theta}_u \|^2_{\mathrm{IP}_*}. \end{aligned}$$

Moreover, similar to (4.3), we can deduce that there is a constant $\epsilon > 0$ with

$$\epsilon \| \widetilde{e}_u \|^2_{L^2(\Omega)} + \epsilon \| \widetilde{e}_u \|^2_{\mathrm{IP}} \leq \widetilde{a}_h(\widetilde{e}_u, \widetilde{e}_u)$$

allowing us to absorb the corresponding right-hand side terms. Integration with respect to time, integration by parts, and exploiting that $\widetilde{e}_u(0) = 0$, give the desired result. □

In addition, utilizing the convergence properties of $\widetilde{\theta}_u$ and the triangle inequality yields

Theorem 5.3 *If u is $(k+1)$-regular with $\partial_t u \in L^2(0, T; H^r(\Omega^\ell \cup \Omega^{\mathrm{g}}))$ for some $0 \leq r \leq k+1$,*

$$\begin{aligned} &\| u - u_h \|^2_{L^\infty(0,T;L^2(\Omega))} + \int_0^T \| u - u_h \|^2_{\mathrm{IP}} \, ds \\ &\quad \leq C \left[h^{2r} |\partial_t u|^2_{L^2(0,T;H^r(\Omega^\ell \cup \Omega^{\mathrm{g}}))} + h^{2k} |u|^2_{L^2(0,T;H^{k+1}(\Omega^\ell \cup \Omega^{\mathrm{g}}))} \right] \end{aligned}$$

This implies convergence of order at least $\min\{r, k\}$ in the $L^\infty(L^2)$ norm.

5.2 Arguments Based on Global L^2 Projection

Clearly, Theorem 5.3 is not optimal due to the high regularity assumption with respect to $\partial_t u$ which naturally cancels by an orthogonality argument of the L^2 projection in the DG case, cf. [25, Proof of Thm. 4.11]. Hence, we mimic this property and achieve $\int_\Omega \frac{1}{\mathcal{H}} \widetilde{\theta}_u \widetilde{e}_u \, d\mathbf{x} = 0$ by defining the L^2 projection to the EG space via

$$\boldsymbol{\pi}' : L^2(\Omega) \to V_m^k, \quad \widetilde{u} \mapsto \boldsymbol{\pi}' \widetilde{u} \quad \text{sufficing} \quad \int_\Omega \tfrac{1}{\mathcal{H}} \boldsymbol{\pi}' \widetilde{u} \widetilde{\varphi} \, d\mathbf{x} = \int_\Omega \tfrac{1}{\mathcal{H}} \widetilde{u} \widetilde{\varphi} \, d\mathbf{x} \quad \forall \widetilde{\varphi} \in V_m^k.$$

This allows us to repeat the arguments of Sect. 5.1 and receive an optimal (also in regularity preconditions) convergence result for the parabolic case. Note that this is a well-defined projection (in contrast to $\boldsymbol{\pi}$) that cannot be (easily) localized to single elements. However, it is a useful tool for our analysis purposes and a natural choice for implementation, since choosing

$$\widetilde{u}_h(0) = \boldsymbol{\pi}' \widetilde{u}_0$$

corresponds to the approach of using integrals of the form $\int_\Omega \frac{1}{\mathcal{H}} \widetilde{u}_0 \widetilde{\varphi} \, d\mathbf{x}$ to create the initial vector of unknowns. It obviously has the best standard L^2 approximating property up to a constant $C > 0$ solely depending on $\mathcal{H}$. Thus for all $v \in L^2(\Omega)$

$$\| \widetilde{v} - \boldsymbol{\pi}' \widetilde{v} \|_{L^2(\Omega)} \leq C \| \widetilde{v} - \boldsymbol{\pi} \widetilde{v} \|_{L^2(\Omega)}. \tag{5.2}$$

This allows us to reprove Lemma 5.2 and Theorem 5.3 by means of $\widetilde{e}'_u$ and $\widetilde{\theta}'_u$ being

$$\widetilde{e}'_u := \widetilde{u}_h - \boldsymbol{\pi}'\widetilde{u} \qquad \text{and} \qquad \widetilde{\theta}'_u = \boldsymbol{\pi}'\widetilde{u} - \widetilde{u},$$

but we additionally have to assume that our mesh sequence is quasi-uniform, i.e. that there is a constant $\rho' > 0$ such that for all $h > 0$ the inequality $h_{\mathcal{K}} \geq \rho' h$ holds for all $\mathcal{K} \in \mathcal{T}_h$. This prevents adaptive refinement which is possible in the previous version of the following results. Thus, we obtain

Lemma 5.4 (Lemma 5.2 revisited) *For almost every $t \in (0, T)$, we have*

$$\|\widetilde{e}'_u(t)\|^2_{L^2(\Omega)} + \int_0^t \|\widetilde{e}'_u(s)\|^2_{\mathrm{IP}}\, ds \leq C \int_0^t \|\widetilde{\theta}'_u(s)\|^2_{\mathrm{IP}*}\, ds.$$

Proof The proof is the same as for Lemma 5.2, but uses $\int_\Omega \frac{1}{\mathcal{H}} \partial_t \widetilde{\theta}'_u \widetilde{e}'_u \, d\mathbf{x} = 0$. □

Theorem 5.5 (Theorem 5.3 revisited) *If u is $(k+1)$-regular and $(\mathcal{T}_h)_h$ is quasi-uniform,*

$$\|u - u_h\|^2_{L^\infty(0,T;L^2(\Omega))} + \int_0^T \|u - u_h\|^2_{\mathrm{IP}}\, ds \leq Ch^{2k} |u|^2_{L^2(0,T;H^{k+1}(\Omega^\ell \cup \Omega^{\mathrm{g}}))}$$

This implies convergence of order at least k in the $L^\infty(L^2)$ norm and does not need any additional regularity.

Proof We have to show that

$$\|\widetilde{\theta}'_u\|_{\mathrm{IP}*} \leq Ch^k |u|_{H^{k+1}(\Omega^\ell \cup \Omega^{\mathrm{g}})}$$

for almost every $t \in (0, T)$. By employing (4.1), it is sufficient to show that

$$|\widetilde{u} - \boldsymbol{\pi}'\widetilde{u}|_{H^r(\mathcal{T}_h)} \leq Ch^{k+1-r} |u|_{H^{k+1}(\Omega^\ell \cup \Omega^{\mathrm{g}})},$$

which can be shown analogously to [8, Lemma 1.58], i.e.

$$\begin{aligned} |\widetilde{u} - \boldsymbol{\pi}'\widetilde{u}|_{H^r(\mathcal{T}_h)} &\leq |\widetilde{u} - \boldsymbol{\pi}\widetilde{u}|_{H^r(\mathcal{T}_h)} + |\boldsymbol{\pi}\widetilde{u} - \boldsymbol{\pi}'\widetilde{u}|_{H^r(\mathcal{T}_h)} \\ &\leq |\widetilde{u} - \boldsymbol{\pi}\widetilde{u}|_{H^r(\mathcal{T}_h)} + C' h^{-r} \|\boldsymbol{\pi}\widetilde{u} - \boldsymbol{\pi}'\widetilde{u}\|_{L^2(\mathcal{T}_h)} \\ &\leq Ch^{k+1-r} |u|_{H^{k+1}(\Omega^\ell \cup \Omega^{\mathrm{g}})}, \end{aligned}$$

where the second inequality follows from the inverse inequality [8, Lemma 1.44] and the third follows from (5.2) and the convergence properties of $\boldsymbol{\pi}$. □

6 Numerical Results

In this section, several numerical results illustrating the performance of our proposed methods are presented. First, an example with constant functions with a jump is tested in Sect. 6.1, then error convergence rate studies for an elliptic problem and a parabolic problem are presented in Sects. 6.2 and 6.3, respectively. Moreover, several scenarios with heterogeneous coefficients are simulated in Sect. 6.4 and curved interfaces are investigated in Sect. 6.5. All computations presented in this work are coded by the authors based on the C++ finite element library deal.II [2].

For the parabolic problem described in Sect. 5, we introduce the notations and algorithm briefly for temporal discretization. The partition of the time interval is defined as

$$0 = t_0 < t_1 < \cdots < t_n < \cdots < t_N = T,$$

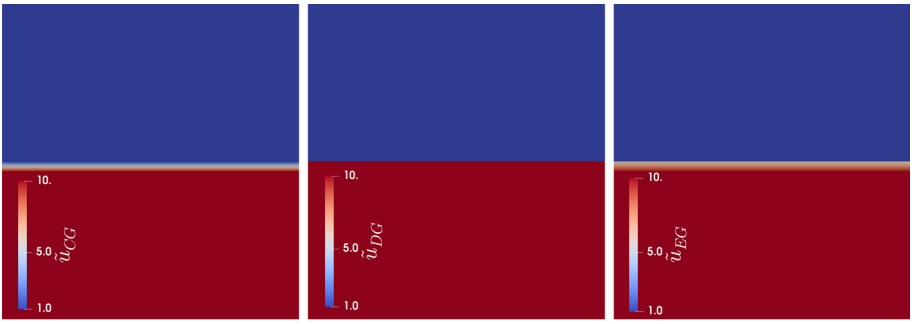

(a) CG **(b)** DG **(c)** EG

Fig. 1 Example 6.1. Post-processed solutions u_h from CG, DG, and EG method, respectively

where $N \in \mathbb{N}$ denotes the total number of time steps. Throughout this section, the backward Euler scheme is utilized for the discretization. For instance, the time derivative term in Definition 5.1 at the given time is discretized via

$$\partial_t u(\cdot, t_n) \approx \frac{u^n - u^{n-1}}{\Delta t}$$

where $u^n := u(t_n)$ and $\Delta t := t_n - t_{n-1}$ denotes the time step size.

6.1 Constant Solutions

In this first example, we test the simple case where two different constant values are considered as the solution for each of the two different parts of the domain. That is, in the computational domain $\Omega = [0, 1]^2$, two domains are separated as $\Omega^\ell = (0, 1) \times (0, 0.5)$ and $\Omega^g = (0, 1) \times (0.5, 1)$ and the solution is given as

$$u_h = \begin{cases} 10 & \text{if } y < 0.5, \\ 1 & \text{other wise,} \end{cases} \quad \text{with} \quad D = \begin{cases} 0.1 & \text{if } y < 0.5, \\ 1 & \text{other wise,} \end{cases}$$

for the elliptic problem (2.1). Then, the right hand side function f and the homogeneous Dirichlet boundary conditions are chosen accordingly to the given solution. Here, we employ the local scheme with

$$\mathcal{H} = \begin{cases} 1 & \text{in } \Omega^\ell \\ H^{\Gamma_{\mathrm{LG}}} & \text{in } \Omega^g, \end{cases} \tag{6.1}$$

where $H^{\Gamma_{\mathrm{LG}}}$ is 10.

The order of polynomial is set to 1 ($k = 1$ and $m = 0$ for the EG scheme) in this case and the results of the post-processed solution u_h for three different discretizations including continuous Galerkin (CG), discontinuous Galerkin (DG), and enriched Galerkin (EG) methods are presented in Fig. 1. The degrees of freedom for CG, DG, and EG in this problem are 1089, 4096, and 2113, respectively. In addition, SIP-DG(EG) is chosen with $\mu = -1$, the interior penalty coefficient is set to be $\eta = 100$, and the minimum mesh size is $h = 0.03125$.

The results illustrate the major two advantages of the proposed scheme. First, it is possible to present the discontinuity in the solution by employing the continuous Galerkin method, which has fewest degrees of freedom and is simplest to implement. Secondly, the enriched

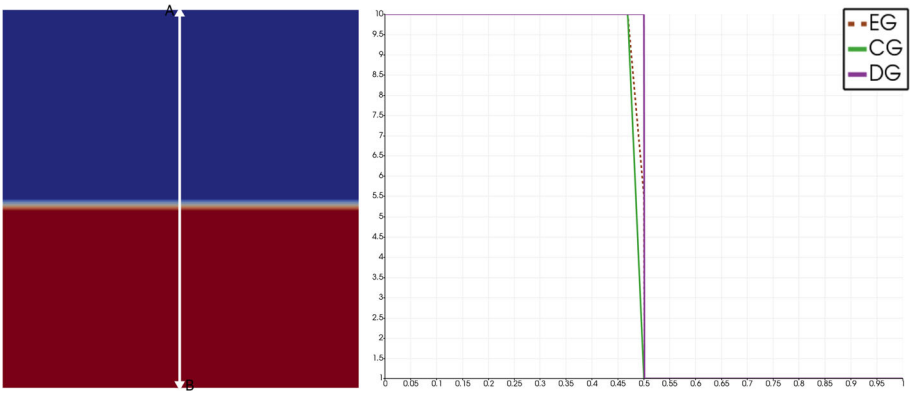

Fig. 2 Example 6.1. Comparison of the CG, DG, and EG solutions plotted on the line $A(0.5, 1) - B(0.5, 0)$. The smearing effects on the interface are solely due to the plotting

Galerkin method (with $m = 0$) also robustly captures the discontinuity and preserves the local mass conservation with fewer degrees of freedom than the discontinuous Galerkin methods.

In addition, the comparison of the solution value (u_h) over the line $(0.5, 0) - (0.5, 1)$ for CG, DG, and EG is illustrated in Fig. 2. Note that the post-processed solutions u_h of the CG and EG methods are forced to be continuous on the interface Γ_{LG} for the plotting. This is due to the construction of the degrees of freedom as nodes of the elements. Thus, the post-processing scheme has to decide whether it divides by $H^{\Gamma_{\mathrm{LG}}}$ or not at the interface Γ_{LG} creating the observed *artificial smearing* effect for the plotting. Although the calculated solution $\widetilde{u}_h$ from our algorithm is accurate, that is why, the continuation of u_h is only for the presentation (plotting) of the solutions.

6.2 Error Convergence Test for the Elliptic Problem

In this example, we study the error convergence rate of the elliptic problem (2.1) without the time derivative term, where the exact solution and the coefficients are given as

$$u_h = \begin{cases} 10\cos x \cos y, & \text{and} \quad D = 0.1, \quad \text{if } y < 0.5 \text{ i.e. in } \Omega^{\ell} \\ \cos x \cos y, & \text{and} \quad D = 1, \quad \text{if } y \geq 0.5 \text{ i.e. in } \Omega^{\mathrm{g}}. \end{cases} \tag{6.2}$$

Here, the computational domains (Ω^{ℓ} and Ω^{g}) are defined as same as the previous example. The Dirichlet boundary conditions are applied for $\partial\Omega$ and the right hand side f is chosen appropriately.

Six computations on uniform meshes were computed where the mesh size h is divided by two for each cycle. The behavior of the $H^1(\Omega)$ semi norm and $L^2(\Omega)$ norm errors for the approximated solution versus the mesh size h are illustrated. Different choices for μ (IIP, NIP, and SIP) were studied, but here the case with $\mu = -1$ (SIP-DG(EG)) and the interior penalty coefficient $\eta = 100$ is shown for the simplicity of the presentation.

We note that the error of the approximated solution $\widetilde{u}_h$, which is the solution before the post-processing is computed here. The computation of the error for post-processed solution u_h requires careful choice due to the *artificial smearing* effect as discussed in the previous section. For example, if the part of the solution is computed with continuous finite elements (CG/EG), the post processing of the solution values on the elements adjacent to Γ_{LG} becomes

Table 1 Example 6.2: The number of degrees of freedom for each of the methods where the maximum polynomial degree is one (with $k = 1$ and $m = 0$ for EG)

Cycle	CG	DG	EG
0	9	16	13
1	25	64	41
2	81	256	145
3	289	1024	545
4	1089	4096	2113
5	4225	16,384	8321

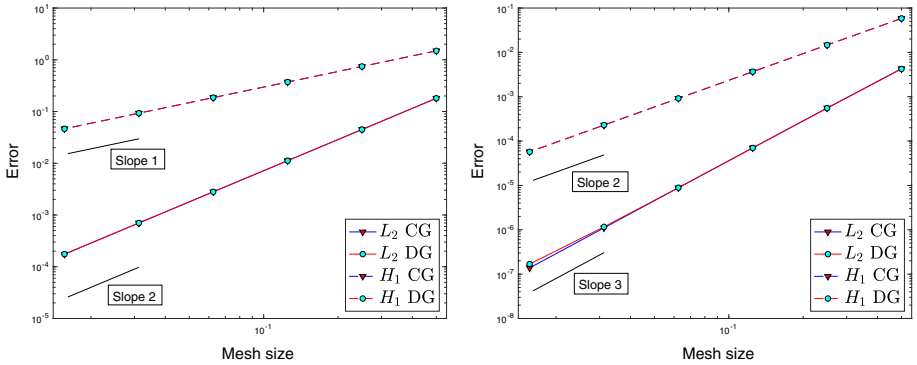

(a) $k = 1$ **(b)** $k = 2$

Fig. 3 Example 6.2: Convergence of the L^2 and H^1 errors of CG and DG for both $k = 1$ (left) and $k = 2$ (right)

an issue for evaluating values. In particular, the post-processing step on the Γ_{LG}, where we divide by H_{LG}, is non-trivial since actual double valued solution from our construction has only one value on Γ_{LG} for CG/EG.

First, Table 1 shows the difference in the number of degrees of freedom (DOF) for each methods. Then, Fig. 3 illustrates both linear $k = 1$ and quadratic orders $k = 2$ for CG and DG. It is observed that the errors are almost identical between CG, DG, and EG methods for this problem. However, it is emphasized that EG (with $m = 0$) has fewer degrees of freedom than that of DG but preserves many advantages of DG [20,21] such as local mass conservation.

Moreover, Fig. 4 presents the error of the solutions of EG with five different cases, where $1 \leq k \leq 2$ and $0 \leq m \leq 2$. In particular, there are the cases for $(k = 1, m = 0)$, $(k = 1, m = 1)$, $(k = 2, m = 0)$, $(k = 2, m = 1)$, and $(k = 2, m = 2)$. The expected optimal orders of convergences as discussed in previous sections are observed. Note that the magnitude of the errors do not depend on the choice of the polynomial order m for EG methods. Thus, for any chosen k values, the optimal choice for m is 0 for this case. This result also corresponds to the analysis shown in the previous section as discussed in Remark 4.9. Currently, the effects and the advantages for considering $m > 0$ for hyperbolic equations (shallow-water) and wave equations are under investigation [30].

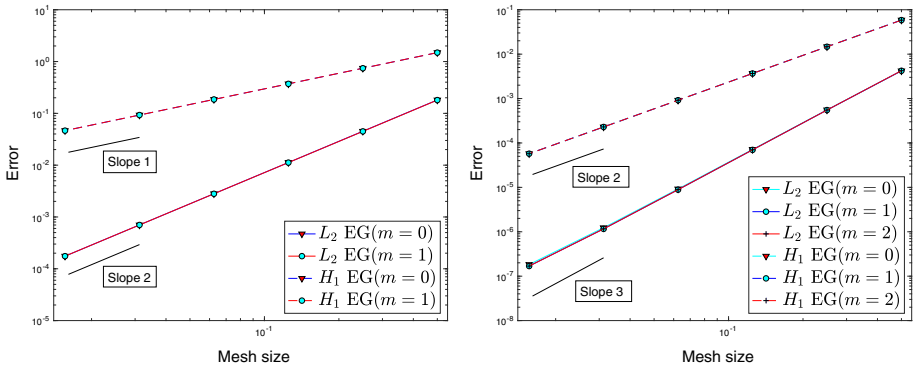

(a) $k = 1$ **(b)** $k = 2$

Fig. 4 Example 6.2. Convergence of the L^2 and H^1 errors of EG methods. (Left) case where $k = 1$ and $m = 0$ or $m = 1$. (Right) case where $k = 2$ and $m = 0$, $m = 1$, or $m = 2$

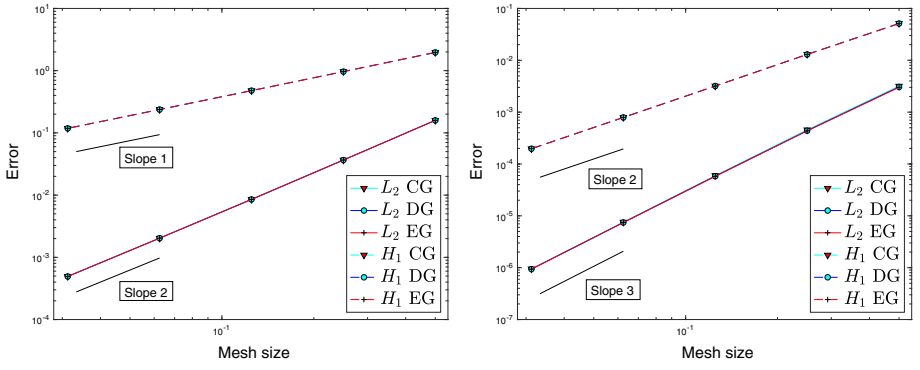

(a) $k = 1$ **(b)** $k = 2$

Fig. 5 Example 6.3. Convergence of the L^2 and H^1 errors for CG, DG, and EG methods. **a** shows the linear case (with $k = 1$ and $m = 0$ for EG); **b** shows the quadratic case (with $k = 2$ and $m = 0$ for EG). The absolute size of the errors for each CG, DG, and EG are almost identical

6.3 Error Convergence Test for the Parabolic Problem

In this example, we extend the previous section, and we present the error convergence of the parabolic problem (5.1) with the time derivative term. The exact solution and coefficients are given as

$$u_h = \begin{cases} 10\cos(t + x - y), & D = 0.1, \quad \text{if } y < 0.5 \text{ i.e. in } \Omega^{\ell} \\ \cos(t + x - y), & D = 1, \quad \text{if } y \geq 0.5 \text{ i.e. in } \Omega^{\mathrm{g}}. \end{cases} \tag{6.3}$$

The computational domains (Ω^{ℓ} and Ω^{g}) are also defined as in the previous example, but the right hand side f and the boundary conditions are chosen appropriately to this problem. Again, we note that the error of the approximated solution $\widetilde{u}_h$, which is the solution before the post-processing is computed here as discussed in the previous sections.

Five computations on uniform meshes were computed where the mesh size h is divided by two for each cycle. The behavior of the $H^1(\Omega)$ semi norm and $L^2(\Omega)$ norm errors for the

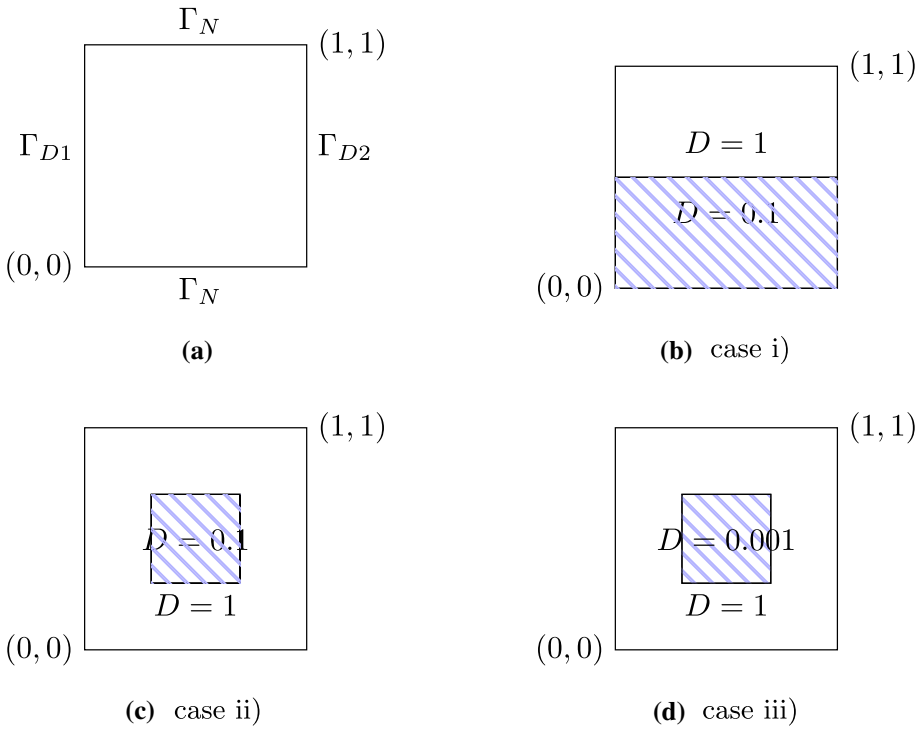

Fig. 6 Example 6.4. Setup. **a** illustrates the computational domain with boundaries. **b**, **c**, and **d** presents the coefficient D values for each cases

approximated solution versus the mesh size h are illustrated for CG, DG, and EG methods. The time discretization is chosen fine enough not to influence the error and also time step size Δt is divided by two for each cycle. The number of time steps for each cycle is 10, 20, 40, 80 and 160. Both linear and quadratic order were tested (with $m = 0$ in the EG case) and the optimal orders of convergence as discussed in previous sections are observed. See Fig. 5. Here, $\mu = -1$ for SIP-DG(EG) and the interior penalty coefficient is set to $\eta = 100$.

6.4 Solutions in Heterogeneous Media

In this example, we solve the parabolic problem (5.1) for the transition of *pressure* solution values in the heterogeneous domain $\Omega = [0, 1]^2$. See Fig. 6 for the setup and the boundary conditions.

Here, three different cases are tested as illustrated in Fig. 6b and c. First, the case i) considers the following coefficient values:

$$D = \begin{cases} 0.1, & \text{if } y < 0.5, \quad \Omega^{\ell} \\ 1, & \text{if } y \geq 0.5, \quad \Omega^{\mathrm{g}} \end{cases} \tag{6.4}$$

and the boundary conditions are chosen as

$$u_D = \begin{cases} 10, & \text{if } y < 0.5 \text{ on } \Gamma_{D1} \times [0, T], \\ 1, & \text{if } y \geq 0.5 \text{ on } \Gamma_{D1} \times [0, T]. \end{cases} \quad u_D = 0 \text{ on } \Gamma_{D2} \times [0, T],$$

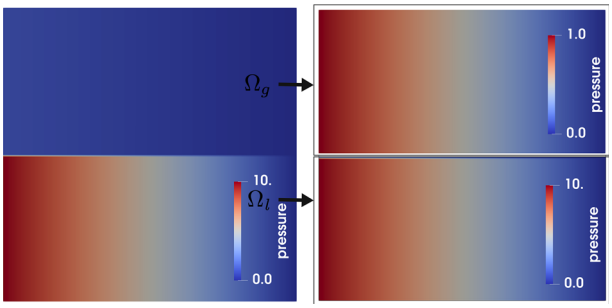

Fig. 7 Example 6.4. case i) Solution values for CG at the time step $n = 500$. The (left) figure shows the solution values on the entire domain Ω and the (right) figure illustrates the two domains Ω^{ℓ} and Ω^{g} separately with different scales

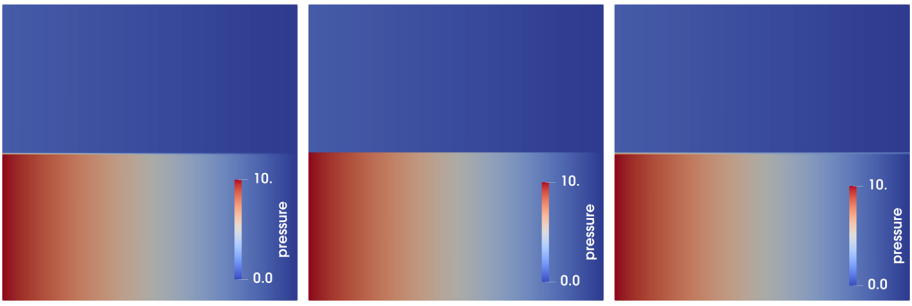

(a) CG **(b)** DG **(c)** EG

Fig. 8 Example 6.4. case i) Solution values for CG, DG, and EG methods, respectively, at the time step $n = 500$

$$\text{and } \frac{\partial u}{\partial n} = 0 \text{ on } \Gamma_N \times [0, T].$$

Here, the final time is set as $T = 5$, the time step size is $\Delta t = 0.01$, and the mesh size is $h = 0.008$. The initial conditions for the solution is zero, i.e $u_0 = 0$.

Case i: First, Fig. 7 presents the solution values (e.g pressure) u_h for the CG method. In particular, the solutions in Ω^{ℓ} and Ω^{g} are separated to take their own scales at the final time step $n = 500$ (see Fig. 7(right)). Figure 8 illustrates and compares the solution values u_h at the final time step, $n = 500$, for each CG, DG, and EG methods. Again, we note that the solution u_h of CG and EG method is forced to be continuous on the interface due to it's construction of degrees of freedom for plotting the solutions on nodal points of the elements. However, this continuation is only for the presentation of the solutions.

Case ii: Next, the case ii) is tested by the following coefficient value

$$D = \begin{cases} 0.1, & \text{if } 0.25 < x < 0.75 \text{ and } 0.25 < y < 0.75, \\ 1, & \text{others}, \end{cases} \tag{6.5}$$

as shown in Fig. 6c. The boundary conditions are chosen as

$$u_D = 1 \text{ on } \Gamma_{D1} \times [0, T], \quad u_D = 0 \text{ on } \Gamma_{D2} \times [0, T],$$
$$\text{and } \frac{\partial u}{\partial n} = 0 \text{ on } \Gamma_N \times [0, T].$$

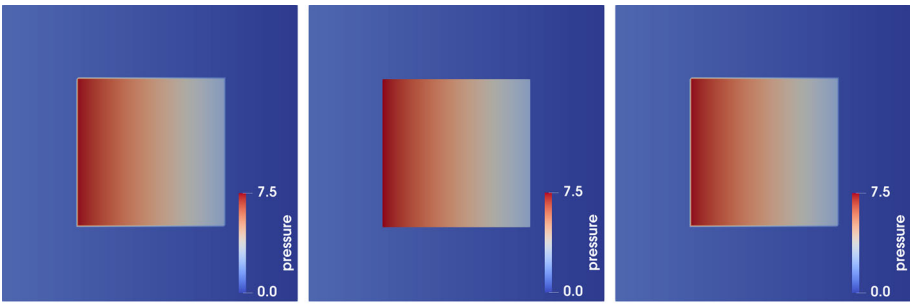

(a) CG **(b)** DG **(c)** EG

Fig. 9 Example 6.4. case ii) Solution values for CG, DG, and EG methods, respectively, at the time step $n = 500$. The smearing effects near the interfaces are solely due to the plotting

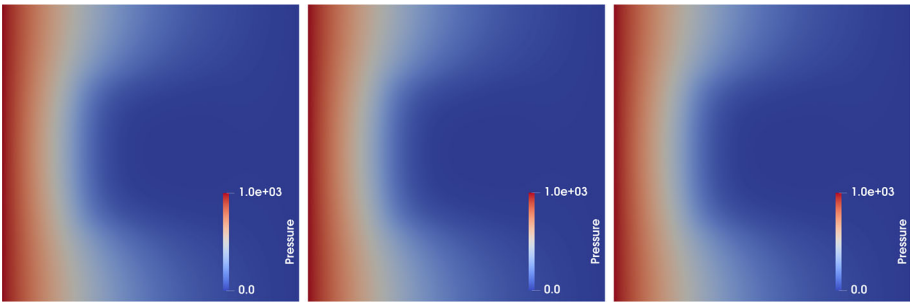

(a) CG **(b)** DG **(c)** EG

Fig. 10 Example 6.4. case iii) Solution values $\widetilde{u}_h$ for CG, DG, and EG methods, respectively, at the time step $n = 500$. The solutions are identical

where $T = 5$ is the final time, the time step size $\Delta t = 0.01$ and the mesh size is $h = 0.008$. The initial conditions for the solution is zero, i.e $u_0 = 0$. Figure 9 illustrates the post-processed solution u_h at the final time, where $n = 500$. The solutions are almost identical for different choices (CG, DG, and EG).

Case iii: The last case iii) has the same condition as the case ii) but with different ratio for the coefficient value, where

$$D = \begin{cases} 0.001, & \text{if } 0.25 < x < 0.75 \text{ and } 0.25 < y < 0.75, \\ 1, & \text{others}, \end{cases} \tag{6.6}$$

as shown in Fig. 6d. Thus, the ratio between the values of D increased to 1000. First, Fig. 10 illustrates and compares the solution values $\widetilde{u}_h$ at the final time step, $n = 500$, for each CG, DG, and EG methods. The comparison of the solutions over the line $0.2 \leq x \leq 0.5$, $y = 0.5$ is presented in the Fig. 12a and we observe the expected identical solutions.

Next, Fig. 11 compares the post-processed solution values u_h at the final time step, $n = 500$, for each CG, DG, and EG methods. The comparison of the solutions over the line $0.2 \leq x \leq 0.5$, $y = 0.5$ is presented in the Fig. 12b. In Fig. 11, we also observe the *artificially smeared* solutions for CG and EG cases, and it is shown in Fig. 12b that it is due to the linear plotting on Γ_{LG}. In particular, the actually double valued solution has only one value on Γ_{LG} and is continuously extended.

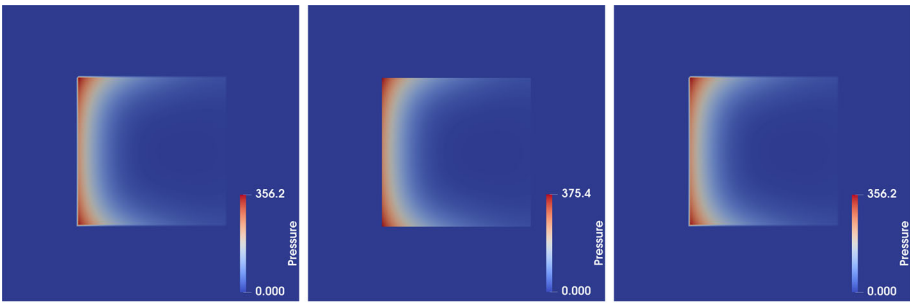

(a) CG **(b)** DG **(c)** EG

Fig. 11 Example 6.4. case iii) Post-processed solution values u_h for CG, DG, and EG methods, respectively, at the time step $n = 500$

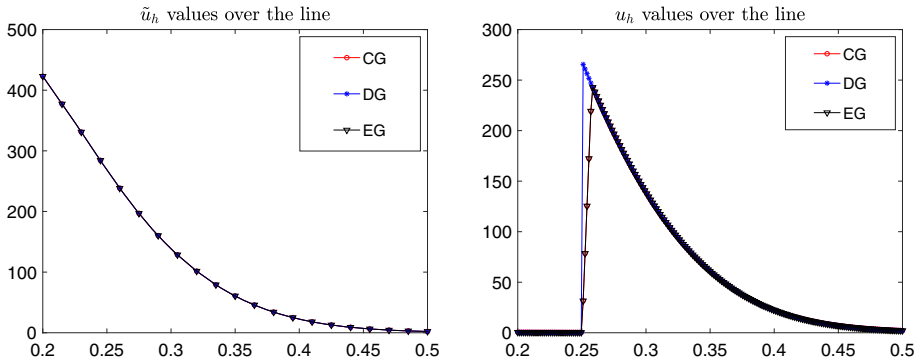

(a) $\widetilde{u}_h$ **(b)** u_h

Fig. 12 Example 6.4. case iii) Solutions plotted over the line $0.2 \leq x \leq 0.5$, $y = 0.5$ at the time step $n = 500$. **a** $\widetilde{u}_h$ for CG, DG, and EG methods. **b** Post-processed solution values u_h for CG, DG, and EG methods, respectively, at the time step $n = 500$. We observe the difference between CG (EG) and DG solutions although the actual solutions are identical. The plotting issues arise where CG (EG) share the degrees of the freedom on the Γ_{LG}, and thus the solution is continuously extended for only plotting. This results to observe the *artificially smeared* solutions for CG and EG cases (see Fig. 11)

6.5 Time Dependent Solution with the Curved Interface

In this final example, we solve the time dependent parabolic problem (5.1) for the transition of the pressure solution values in the heterogeneous domain $\Omega = [0, 1]^2$. The difference in this example compared to the previous one is that here we test the curved interface to emphasize the capability of our proposed algorithm.

First, all the numerical and physical parameters, and the boundary conditions including the computational domain are the same as the previous example. However, the subdomain for Ω^{ℓ} is differently defined by considering three small circular subdomains Ω^{ℓ_i} $(i = 1, 2, 3)$ such as

$$\Omega^{\ell_1} := \{(x, y) \in \Omega | \sqrt{(x - 0.35)^2 + (y - 0.725)^2} < 0.125\},$$

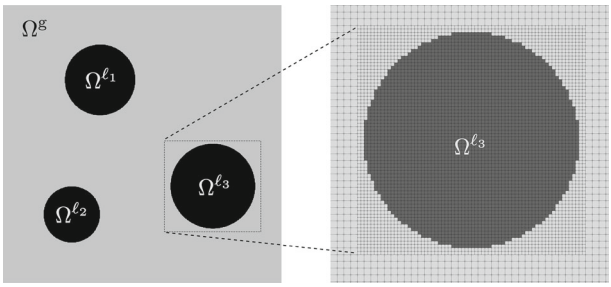

Fig. 13 Example 6.5. Setup. Here $\Omega^{\ell} = \Omega^{\ell_1} \cup \Omega^{\ell_2} \cup \Omega^{\ell_3}$ and we adaptively refine more near Ω^{ℓ} for better resolution of the curves

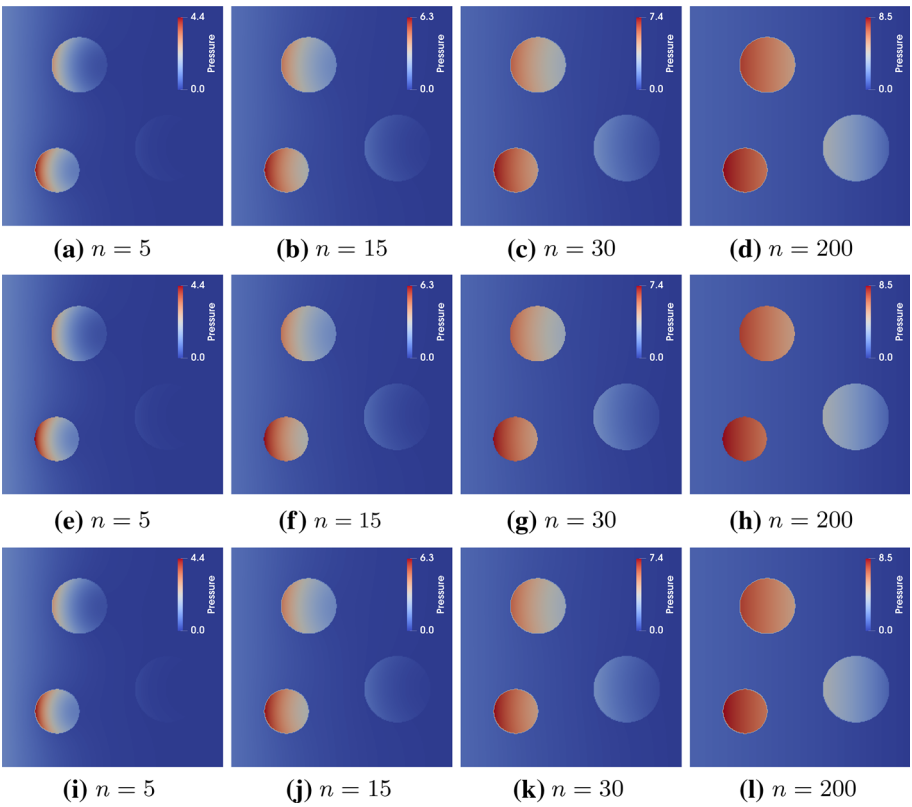

(a) $n = 5$ **(b)** $n = 15$ **(c)** $n = 30$ **(d)** $n = 200$

(e) $n = 5$ **(f)** $n = 15$ **(g)** $n = 30$ **(h)** $n = 200$

(i) $n = 5$ **(j)** $n = 15$ **(k)** $n = 30$ **(l)** $n = 200$

Fig. 14 Example 6.5. Solution values for CG (top), DG (middle), and EG (bottom) for each time step $n = 5, 15, 30$, and 200

$$\Omega^{\ell_2} := \{(x, y) \in \Omega | \sqrt{(x - 0.25)^2 + (y - 0.25)^2} < 0.1\},$$
$$\Omega^{\ell_3} := \{(x, y) \in \Omega | \sqrt{(x - 0.75)^2 + (y - 0.35)^2} < 0.15\}$$

with

$$D = \begin{cases} 0.1 & \text{in } \Omega^{\ell}, \\ 1 & \text{in } \Omega^{\mathrm{g}}. \end{cases} \tag{6.7}$$

See Fig. 13 for the detailed setup and mesh refinement near the curve for better resolution.

Figure 14 presents the solution values u_h for CG, DG, and EG methods for different time steps, $n = 5, 15, 30,$ and 200 and shows the expected behavior. The solution values are all identical. However, any rigorous numerical analyses with the curved interface is not trivial with our setup yet. This is an ongoing study.

7 Conclusion and Future Prospects

In this article, we constructed a CG, a DG, and an EG scheme to deal with a diffusion equation in which the primary unknown satisfies a jump condition (Henry's law) at a predefined interface. Moreover, we analyzed all three schemes in a unified fashion and recognized that the order of convergence only depends on the maximum polynomial degree of the approximation spaces. This is underlined by numerical experiments also suggesting that the total L^2 and H^1 errors depend almost exclusively on the maximum polynomial degree (independent of the fact whether this is related to the continuous or discontinuous approximation space). This indicates that the computationally most performant choice is CG. It is sufficient to enrich CG by piecewise constants to ensure local mass conservation. However, enrichment (especially by higher order polynomials) does not (significantly) decrease the error (but significantly increases computational costs).

Possible future research areas in this direction include conducting further comparisons among CG, DG, and EG for curved interfaces by extending our uniform approach of numerical analyses. Ongoing works include considering other physics or equations where the enrichment with $m > 0$ is necessary to construct stable higher order schemes.

Acknowledgements A. Rupp acknowledges financial support by the Deutsche Forschungsgemeinschaft (DFG, German Research Foundation) under Germany's Excellence Strategy EXC 2181/1 - 390900948 (the Heidelberg STRUCTURES Excellence Cluster). S. Lee is supported by the National Science Foundation under Grant No. (NSF DMS-1913016).

References

1. Abels, H., Garcke, H., Grün, G.: Thermodynamically consistent, frame indifferent diffuse interface models for incompressible two-phase flows with different densities. Math. Models Methods Appl. Sci. 1150013-1–1150013-40 (2012)
2. Arndt, D., Bangerth, W., Clevenger, T.C., Davydov, D., Fehling, M., Garcia-Sanchez, D., Harper, G., Heister, T., Heltai, L., Kronbichler, M., Kynch, R.M., Maier, M., Pelteret, J.-P., Turcksin, B., Wells, D.: The `deal.II` library, version 9.1. J. Numer. Math. (2019, accepted). https://doi.org/10.1515/jnma-2019-0064. https://dealii.org/deal91-preprint.pdf
3. Becker, R., Burman, E., Hansbo, P., Larson, M.G.: A reduced P1-discontinuous Galerkin method. Chalmers Finite Element Center Preprint 2003-13 (2003)
4. Chabaud, B., Cockburn, B.: Uniform-in-time superconver-gence of HDG methods for the heat equation. Math. Comput. **81**, 107–129 (2012)
5. Chen, Z., Zou, J.: Finite element methods and their convergence for elliptic and parabolic interface problems. Numerische Mathematik **79**, 175–202 (1998). https://doi.org/10.1007/s002110050336
6. Choo, J., Lee, S.: Enriched Galerkin finite elements for coupled poromechanics with local mass conservation. Comput. Methods Appl. Mech. Eng. **341**, 311–332 (2018)
7. Chu, C.-C., Graham, I., Hou, T.-Y.: A new multiscale finite element method for high-contrast elliptic interface problems. Math. Comput. **79**, 1915–1955 (2010)
8. Di Pietro, D.A., Ern, A.: Mathematical Aspects of Discontinuous Galerkin Methods, Mathmatiques et Applications. Springer, Heidelberg (2012)

9. Ern, A., Guermond, J.-L.: Theory and Practice of Finite Elements, Applied Mathematical Sciences. Springer, New York (2004)
10. Huang, J., Zou, J.: Some new a priori estimates for second-order elliptic and parabolic interface problems. J. Differ. Equ. **184**, 570–586 (2002)
11. Jäger, W., Mikelić, A., Neuss-Radu, M.: Analysis of differential equations modelling the reactive flow through a deformable system of cells. Arch. Ration. Mech. Anal. **192**, 331–374 (2009). https://doi.org/10.1007/s00205-008-0118-4
12. Kadeethum, T., Nick, H., Lee, S.: Comparison of two-and three-field formulation discretizations for flow and solid deformation in heterogeneous porous media. In: 20th Annual Conference of the International Association for Mathematical Geosciences (2019)
13. Kadeethum, T., Nick, H., Lee, S., Richardson, C., Salimzadeh, S., Ballarin, F.: A novel enriched Galerkin method for modelling coupled flow and mechanical deformation in heterogeneous porous media. In: 53rd US Rock Mechanics/Geomechanics Symposium. American Rock Mechanics Association, New York, NY, USA (2019)
14. Kadeethum, T., Nick, H.M., Lee, S., Ballarin, F.: Flow in porous media with low dimensional fractures by employing enriched Galerkin method. Adv. Water Resour. (2020). https://doi.org/10.1016/j.advwatres.2020.103620
15. Knabner, P., Angermann, L.: Numerical Methods for Elliptic and Parabolic Partial Differential Equations, Texts in Applied Mathematics. Springer, New York (2003). https://doi.org/10.1007/b97419
16. Kuzmin, D., Hajduk, H., Rupp, A.: Locally bound-preserving enriched Galerkin methods for the linear advection equation. Comput. Fluids **205**, 15 (2020). https://doi.org/10.1016/j.compfluid.2020.104525
17. Lee, S., Choi, W.: Optimal error estimate of elliptic problems with Dirac sources for discontinuous and enriched Galerkin methods. Appl. Numer. Math. (2019). https://doi.org/10.1016/j.apnum.2019.09.010
18. Lee, S., Lee, Y.-J., Wheeler, M.F.: A locally conservative enriched Galerkin approximation and efficient solver for elliptic and parabolic problems. SIAM J. Sci. Comput. **38**, A1404–A1429 (2016)
19. Lee, S., Mikelic, A., Wheeler, M.F., Wick, T.: Phase-field modeling of two phase fluid filled fractures in a poroelastic medium. Multiscale Model. Simul. **16**, 1542–1580 (2018)
20. Lee, S., Wheeler, M.F.: Adaptive enriched Galerkin methods for miscible displacement problems with entropy residual stabilization. J. Comput. Phys. **331**, 19–37 (2017)
21. Lee, S., Wheeler, M.F.: Enriched Galerkin methods for two-phase flow in porous media with capillary pressure. J. Computat. Phys. **367**, 65–86 (2018)
22. Lehrenfeld, C., Reusken, A.: High Order Unfitted Finite ElementMethods for Interface Problems and PDEs on Surfaces, pp. 33–63. Springer, Cham (2017). https://doi.org/10.1007/978-3-319-56602-3_2
23. Muntean, A., Böhm, M.: A moving-boundary problem for concrete carbonation: global existence and uniqueness of weak solutions. J. Math. Anal. Appl. **350**, 234–251 (2009). https://doi.org/10.1016/j.jmaa.2008.09.044
24. Rupp, A.: Simulating Structure Formation in Soils Across Scales Using Discontinuous Galerkin Methods, Mathematik, Shaker Verlag GmbH. Düren 07 (2019). https://doi.org/10.2370/9783844068016
25. Rupp, A., Knabner, P., Dawson, C.: A local discontinuous Galerkin scheme for Darcy flow with internal jumps. Comput. Geosci. **22**, 1149–1159 (2018). https://doi.org/10.1007/s10596-018-9743-7
26. Rupp, A., Totsche, K.U., Prechtel, A., Ray, N.: Discrete-continuum multiphase model for structure formation in soils including electrostatic effects. Front. Environ. Sci. **6**, 13 (2018). https://doi.org/10.3389/fenvs.2018.00096
27. Sander, R.: Compilation of Henry's law constants (version 4.0) for water as solvent. Atmos. Chem. Phys. **15**, 4399–4981 (2015). https://doi.org/10.5194/acp-15-4399-2015
28. Sochala, P., Ern, A., Piperno, S.: Mass conservative BDF-discontinous Galerkin/explicit finite volume schemes for coupling subsurface and overland flows. Comput. Methods Appl. Mech. Eng. **198**, 2122–2136 (2009). https://doi.org/10.1016/j.cma.2009.02.024
29. Sun, S., Liu, J.: A locally conservative finite element method based on piecewise constant enrichment of the continuous Galerkin method. SIAM J. Sci. Comput. **31**, 2528–2548 (2009)
30. Vamaraju, J., Sen, M., Basabe, J.D., Wheeler, M.: A comparison of continuous, discontinuous, and enriched Galerkin finite-element methods for elastic wave-propagation simulation. pp. 4063–4067 (2017). https://doi.org/10.1190/segam2017-17658225.1